Electronic Supplementary Information

Cost-efficient quinoxaline-based semiconducting polymers: systematic structure–property–morphology correlation toward reliable organic field-effect transistors

Yuta Otake,[a] Atsushi Isobe,[a] Ting-Yu Wang,[b] Chu-Chen Chueh,[b] Masayuki Wakioka,[c] and Tsuyoshi Michinobu[a,*]

[a] *Department of Materials Science and Engineering, Institute of Science Tokyo, 2-12-1 Ookayama, Meguro-ku, Tokyo 152-8552, Japan*

[b] *Department of Chemical Engineering, National Taiwan University, Taipei 10617, Taiwan*

[c] *Sagami Chemical Research Institute, 2743-1 Hayakawa, Ayase, Kanagawa 252-1193, Japan*

E-mail: michinobu@mct.isct.ac.jp

Contents

1. General and Materials

General

^{1}H (400 MHz), ^{13}C (100 MHz), and ^{19}F (376 MHz) NMR spectra were measured on a JEOL JNM-ECZ400S spectrometer at ambient temperature. $CDCl_3$ was used as the solvent, and tetramethylsilane (TMS) was used as an internal standard (δ = 0.00 ppm) for ^{1}H and ^{13}C NMR measurements. For ^{19}F NMR measurements, trifluoroacetic acid (TFA) was used as an internal standard (δ = −76.3 ppm).[S1] Structural assignments were made based on ^{1}H–^{1}H COSY, g-HSQC, g-HMBC, and DEPT-135 NMR experiments. Infrared (IR) spectra were recorded using a JASCO FT/IR-4200 spectrometer with a resolution of 4 cm^{-1}, and absorption bands are reported in wavenumbers (cm^{-1}). Thermogravimetric analysis (TGA) and differential scanning calorimetry (DSC) measurements were carried out on a Rigaku TG8120 and Rigaku DSC8230, respectively. Absorption spectra were measured on a JASCO V-670 spectrometer. Electrochemical measurements using cyclic voltammetry (CV) were performed with a BAS Model 612C electrochemical analyzer with a three-electrode cell. Photoelectron yield spectroscopy (PYS) measurements were performed using an AC-2S spectrometer (Riken Keiki Co., Ltd.) equipped with a deuterium lamp. MALDI-TOF mass spectra were recorded on a Shimadzu MALDI-8030 mass spectrometer equipped with a solid-state laser operating at a wavelength of 355 nm. The laser repetition rate was set to 200 Hz during the measurements. All calculations were conducted using a Gaussian 16 suite program (G16RevC.02).[S2] Geometry optimizations were performed at the ωB97XD/6-31G(d,p) level of theory. Frontier molecular orbital (HOMO and LUMO) and natural bond orbital (NBO) analyses were performed based on the optimized geometries at the same level of theory. For computational efficiency, all alkyl side chains were simplified to methyl groups. Organic field-effect transistor (OFET) devices were characterized using a Keithley 4200-SCS.

Materials

1,2-Diamino-4,5-difluorobenzene and (3,3'-difluoro-[2,2'-bithiophene]-5,5'-diyl)bis(trimethylstannane) were purchased from BLD Pharm. P(*tert*-Bu)$_3$ Pd G3 was purchased from ChemScene. 19-(3-Iodopropyl)heptatriacontane was purchased from Lyntech Co., Ltd. 2,5-Bis(trimethylstannyl)thiophene was purchased from Tokyo Chemical Industry Co., Ltd. (TCI). 2,5-Bis(trimethylstannyl)thieno[3,2-*b*]thiophene and tripotassium phosphate were purchased from Sigma-Aldrich Co., Ltd. Other reagents were purchased from commercial sources and used without further purification. 5,8-Dibromo-6,7-difluoroquinoxalin-2-ol (**Qx-3**) was prepared according to a reported method.[S3] Silica-gel column chromatography was performed using Silica Gel 60 (spherical) and Silica Gel 60N (spherical, neutral) from Kanto Chemical Co., Inc., YAMAZEN Universal Premium L, or Biotage® Sfär Silica D, on a Biotage® Isolera One system equipped with UV–vis detection (250–400 nm).

2. Experimental Procedures

2.1. Measurements

Gel Permeation Chromatography (GPC)

GPC curves, number-average molecular weight (M_n), weight-average molecular weight (M_w), and polydispersity index (PDI; M_w/M_n) of the polymers were measured using a JASCO CO-2065 Plus system equipped with a pump (PU-2080 Plus), a refractive index (RI) detector (RI-2031 Plus), and a UV–vis absorbance detector (UV-2075 Plus, detection wavelength: 600 nm). 1,2-Dichlorobenzene (*o*-DCB) was used as eluent at 40 °C, calibrated using polystyrene standards. Measurements were carried out on two Shodex KF-803 columns (8.0 mm i.d. × 300 mm) at a flow rate of 0.5 mL min^{-1}. Polymer solutions (ca. 1 mg mL^{-1}) were used for analysis.

Matrix-Assisted Laser Desorption/Ionization Time-of-Flight Mass Spectrometry (MALDI-TOF-MS)

For MALDI–TOF MS measurements, samples were prepared using appropriate organic matrices. For polymers **P1**, **P2**, **P4**, and **P6**, chloroform solutions of the polymers (1 mg mL^{-1}) were mixed with matrix solutions (*trans*-2-[3-(4-*tert*-butylphenyl)-2-methyl-2-propenylidene]malononitrile (DCTB) for **P1**, **P2**, and **P4** and dithranol for **P6** in chloroform (20 mg mL^{-1}) at a volume ratio of 1:1 (50 μL each)), followed by sonication to ensure homogeneous mixing. A 1 μL aliquot of each resulting mixture was deposited onto a Shimadzu FleXiMass-SR48 MALDI target plate. For polymers **P3** and **P5**, chloroform solutions of the polymers (1 mg mL^{-1}, 1 μL) were first deposited onto the plate, followed by deposition of 1 μL of matrix solutions (DCTB for **P3** and dithranol for **P5** in chloroform (20 mg mL^{-1}) containing 0.05 vol% TFA). For **Qx-5**, a chloroform solution of the compound (1 mg mL^{-1}, 1 μL) was first deposited onto the plate, followed by deposition of 1 μL of a dithranol matrix solution in THF (10 mg mL^{-1}) containing 0.05 vol% TFA. For all samples, the deposited spots were allowed to dry under ambient conditions for more than 30 minutes prior to measurement.

Thermogravimetric Analysis (TGA)

TGA was performed using approximately 1–2 mg of sample placed in an aluminum pan under a nitrogen purge (500 mL min^{-1}) at a heating rate of 10 °C min^{-1} over a temperature range from 0 to 500 °C.

Differential Scanning Calorimetry (DSC)

DSC measurements were performed using approximately 2–3 mg of sample sealed in an aluminum pan with a lid under a nitrogen purge (150 mL min^{-1}). After determination of the 5% degradation temperature, heating and cooling cycles were carried out over a temperature range from 0 to 300 °C at a heating/cooling rate of 10 °C min^{-1}, starting from room temperature and repeated three times. The second heating and cooling cycles were used to discuss thermal properties.

Absorption Spectra

Film:

Approximately 50–100 μL of a polymer solution in chloroform (0.5–1 mg mL^{-1}) was cast onto a quartz glass substrate (1 cm width) and dried at room temperature for at least 30 min. UV–vis absorption spectra of the as-cast films were measured over the wavelength range of 250–850 nm, and the optical bandgaps

were determined from the as-cast films. Subsequently, the film was thermally annealed at 200 °C or 300 °C for 15 min, and the UV–vis absorption spectra were recorded again over the same wavelength range.

Solution:

UV–vis absorption spectra of the polymer solutions (10^{-5} M in chloroform) were measured using a quartz cuvette over the wavelength range of 250–1000 nm. Temperature-dependent measurements were carried out during both heating and cooling between 15 and 55 °C in 10 °C increments. Spectra were recorded after the temperature was stabilized at each set point.

Photoelectron Yield Spectroscopy (PYS)

The HOMO energy levels of the polymers were estimated using PYS in air. Polymer thin films were prepared on octadecyltrimethoxysilane (OTMS)-modified SiO_2 (300 nm)/Si substrates by spin-coating chloroform solutions of the polymers (4–6 mg mL^{-1}), following the same procedure used for OFET device fabrication. The resulting films were thermally annealed at the optimized temperatures for each polymer prior to measurement. PYS measurements were carried out by irradiating the polymer films with ultraviolet light in the photon energy range from 4.20 to 6.20 eV with an energy step of 0.10 eV. The acquisition time at each photon energy was set to 10 s, and the UV light intensity was controlled in the range of 10–200 nW. The photoelectron yield was plotted as a function of photon energy, and the onset energy for photoemission was determined from the intersection of the baseline and the linear regression line fitted to the rising edge of the yield curve. The HOMO energy levels were estimated by subtracting this onset energy from the vacuum level.

Cyclic Voltammetry (CV)

Electrochemical measurements were performed in acetonitrile (MeCN) containing 0.1 M tetrabutylammonium perchlorate (*n*-Bu_4NClO_4) as the supporting electrolyte. A glassy carbon disk electrode (diameter: 3 mm) was used as the working electrode, a platinum wire as the counter electrode, and an Ag/AgCl electrode as the reference electrode. Prior to measurements, the electrolyte solution was degassed by bubbling argon gas for at least 15 min, and the absence of oxygen-related redox peaks was confirmed. Polymer films were prepared by drop-casting two drops of a chloroform solution of the polymer (1 mg mL^{-1}) onto the working electrode using a Pasteur pipette, followed by drying at room temperature and under a gentle stream of warm air. All electrochemical measurements were conducted at room temperature (ca. 25 °C). CV measurements were carried out at a scan rate of 100 mV s^{-1}. For reduction measurements, the potential was initially scanned from 0.1 V to –2.0 V and then reversed. For oxidation measurements, a freshly prepared polymer film was used, and the potential was scanned from −0.1 V to 2.0 V and then reversed. Ferrocene (Fc) was measured as an external standard using a 0.01 M solution in acetonitrile containing 0.1 M *n*-Bu_4NClO_4 as the supporting electrolyte under the same electrochemical conditions as those used for the polymer measurements. The potential was scanned from 0 V toward the positive direction up to 1.0 V, then reversed to –1.0 V, and finally returned to 0 V at a scan rate of 100 mV s^{-1}. The onset oxidation and reduction potentials were determined from the intersection of the tangent at the rising edge of the redox current with

the baseline. The HOMO and LUMO energy levels were electrochemically estimated from the onset oxidation and reduction potentials obtained by cyclic voltammetry according to the following equations:

$$E_{\mathrm{HOMO}}^{\mathrm{CV}} = -(E_{\mathrm{ox,onset}} - E_{\mathrm{Fc/Fc^+}} + 4.80)\ \mathrm{eV}$$

$$E_{\mathrm{LUMO}}^{\mathrm{CV}} = -(E_{\mathrm{red,onset}} - E_{\mathrm{Fc/Fc^+}} + 4.80)\ \mathrm{eV}$$

Fabrication and Characterization of Organic Field-Effect Transistors

Top-contact bottom-gate (TC/BG) OFETs were fabricated on a heavily n-doped Si wafer (N++-Si) with a thermally grown 300 nm-thick SiO_2 layer ($C_i \approx 11.2$ nF cm^{-2}); the substrates had a typical size of ca. 1.3 cm × 1.3 cm. First, the substrates were sequentially sonicated for 10 min in 50 mL of each solvent, in the order of deionized water, acetone (EL grade), and isopropanol (EL grade), and then dried by blowing nitrogen gas. They were then heated to 120 °C for 10 min to remove residual solvents while being covered with a lid to prevent contamination, and subsequently cooled to room temperature in air. The wafers were then treated with UV-ozone for 20 min. The SiO_2 surface was modified with a self-assembled monolayer (SAM) of OTMS under ambient conditions following a reported procedure.[S4] A syringe-filtered OTMS solution (7.5 μL of OTMS in 5 mL of toluene, filtered through a 0.45 μm membrane filter) was cast (100 μL) onto the UV-ozone-treated substrates. The substrates were kept stationary at 0 rpm for 20 s to allow the OTMS molecules to self-assemble on the surface, followed by spin-coating at 3000 rpm for 40 s. After spin coating, the substrates were placed in a sealed chamber filled with ammonia vapor, which was generated by evacuating the chamber for several seconds in the presence of aqueous ammonia. The substrates were exposed to ammonia vapor under static conditions for at least 12 h. Subsequently, the substrates were removed from the chamber and sequentially sonicated in the order of deionized water followed by toluene, using approximately 50 mL of each solvent for 5 min per solvent. The successful formation of the OTMS SAM was confirmed by the hydrophobic nature of the treated surface.

P1–**P6** were dissolved in anhydrous chloroform (containing amylenes as a stabilizer, ≥ 99%) at a concentration of 4–6 mg mL^{-1}. The polymer solutions were stirred at 40 °C and 400 rpm for at least 12 h in a nitrogen-filled glovebox. After cooling to room temperature, solutions were subsequently filtered through a 0.45 μm syringe filter prior to use. For each substrate, 90 μL of the filtered polymer solution was dispensed, followed by spin-coating at 3000 rpm for 40 s in a glovebox. The resulting films were thermally annealed (as-cast, 100 °C, 200 °C, or 300 °C) for 15 min under a nitrogen atmosphere in the same glovebox.

After spin coating and thermal annealing, the substrates were removed from the glovebox, and gold (Au) source and drain electrodes were deposited by thermal evaporation under vacuum through a shadow mask. The shadow mask, defining a channel length (L) of 100 μm and a channel width (W) of 1 mm, was fixed onto the substrates using polyimide tape. For **P6**-based OFET devices, Au source/drain electrodes with channel lengths (L) ranging from 50 to 200 μm and a channel width (W) of 1 mm were additionally fabricated to investigate parasitic effects using the transfer line method (TLM). The substrates were placed upside down in the evaporation chamber facing the Au source. Prior to deposition, the chamber was evacuated to a base pressure below 3.0×10^{-3} Pa. Au (~50 nm) was thermally evaporated using a resistive

heating source by gradually increasing the current to 70–80 A. The deposition rate was maintained at approximately 0.05 nm s^{-1}, as monitored by a thickness monitor. After reaching the target thickness, the Au source was shielded, and the current was reduced to zero. After cooling to room temperature, the devices were removed from the vacuum chamber and used for measurements. The OFET measurements were performed under different environments depending on the carrier type. p-Type characteristics were measured in air for all devices. For the ambipolar polymer **P6**, both p- and n-type characteristics were additionally measured under vacuum (< 2.0×10^{-2} Pa) on a probe stage, enabling direct comparison under identical conditions. Saturation mobilities were calculated according to the following equation:

$$\sqrt{I_D} = \sqrt{\frac{WC_i\mu}{2L}}(V_G - V_{th})$$

where μ is the field-effect mobility in the saturation regime; W and L are the channel width and length, respectively; C_i is the areal capacitance of the gate dielectric; I_D is the drain current; V_G is the gate voltage; and V_{th} is the threshold voltage.

Two-Dimensional Grazing-Incidence Wide-Angle X-Ray Scattering (GIWAXS) Measurements

GIWAXS measurements were performed at the BL23A beamline of the National Synchrotron Radiation Research Center. Polymer solutions were spin-coated onto OTMS-modified SiO_2 (300 nm)/Si substrates under the same conditions as those used for OFET device fabrication. The X-ray wavelength was 1.2398 Å, and the incident angle was fixed at 0.15°.

Two-dimensional (2D) scattering patterns were collected and converted into one-dimensional (1D) line-cut profiles along the out-of-plane (q_z) and in-plane (q_{xy}) directions using the GIXS Analysis software.[S5] The lamellar (h00) diffraction peaks were analyzed to extract the d-spacing and crystal coherence length (CCL). The diffraction peaks were fitted using Gaussian functions to determine the full width at half maximum (FWHM).

Crystallographic parameters, d-spacing and CCL was estimated using the following equations:[S6]

$$d_{lamellar} = \frac{2\pi}{q_z}$$

$$\mathrm{CCL} = 2\pi K / \mathrm{FWHM}$$

where q_z is the out-of-plane position vector and K is the shape factor (0.90).

Atomic Force Microscopy (AFM) Measurements

AFM measurements were performed using a Seiko Instruments SPA300 system operated in dynamic force microscopy (DFM, tapping) mode under ambient conditions. Silicon cantilevers (DF-20, Seiko Instruments) with a resonance frequency of approximately 124 kHz and a spring constant of 16 N m^{-1} (nominal values), coated with Al, were employed. Height images were acquired over a scan area of 2 μm × 2 μm. Polymer thin films were prepared by spin-coating polymer solutions onto OTMS-modified SiO_2 (300 nm)/Si substrates under the same conditions as those used for OFET device fabrication. The obtained AFM

images were processed as necessary by first-order plane correction, flattening, and fast Fourier transform (FFT) analysis using standard image processing procedures.

2.1. Synthesis

Synthesis of **Qx-4**

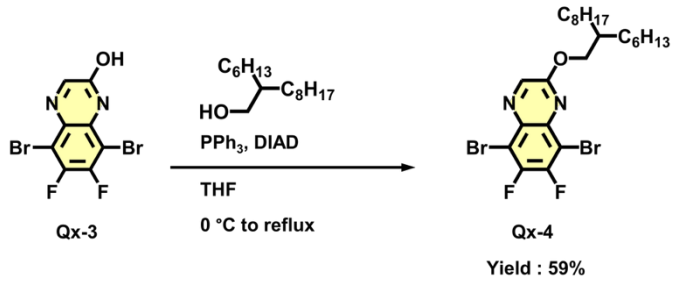

.

Qx-3 (661.9 mg, 1.95 mmol) and triphenylphosphine (111.8 mg, 2.17 mmol) were added to a 300 mL two-necked flask. The atmosphere in the flask was replaced with Ar. Anhydrous THF (63.0 mL) was added to the flask. The reaction mixture was cooled to ca. 0 °C using an ice bath. Then, 2-hexyldecan-1-ol (0.650 mL, 2.25 mmol) was added dropwise to the solution over 1 min, followed by the dropwise addition of diisopropyl azodicarboxylate (40% in toluene) (1.60 mL, 2.98 mmol) over 16 min under cooling. The reaction mixture was subsequently allowed to warm naturally to room temperature. After stirring for 1.5 h, the reaction mixture was heated to reflux and stirred for an additional 19 h. The mixture was then cooled to room temperature, and the solvent was removed under reduced pressure. The resulting residue was dissolved in a minimal amount of dichloromethane, after which approximately 4 g of dry silica gel was added. The solvent was removed under reduced pressure to afford a free-flowing powder, which was purified by flash silica-gel column chromatography. Elution was performed using hexane/dichloromethane (98/2, v/v) for 1 column volume (CV), followed by a gradient from 98/2 to 90/10 (v/v) over 10 CV at a flow rate of 20 mL min^{-1} to afford **Qx-4** (654.8 mg, 1.16 mmol, 59%) as a pale yellow liquid. The chemical shifts of the ^1H NMR spectrum agreed with values reported in the literature.[S3] Spectral data for **Qx-4**: ^1H NMR (400 MHz, $CDCl_3$): $\delta = 8.52$ (s, 1H), 4.49 (d, $J = 5.7$ Hz, 2H), 1.89 (m, 1H), 1.14–1.46 (m, 24H), 0.84–0.94 (m, 6H) ppm.

Synthesis of **Qx-5**

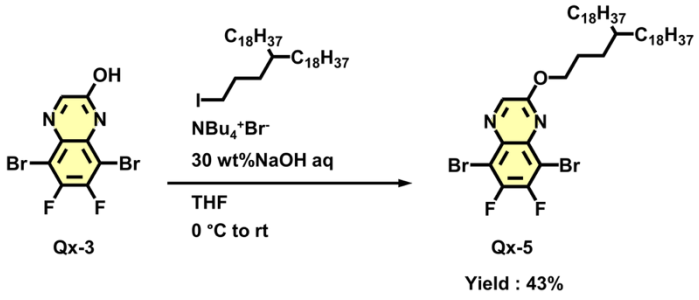

Qx-3 (200.3 mg, 0.589 mmol), tetrabutylammonium bromide (111.8 mg, 0.347 mmol), and 19-(3-iodopropyl)heptatriacontane (1.230 g, 1.78 mmol) were added to a 100 mL two-necked flask. The atmosphere in the flask was replaced with Ar. THF (8.0 mL) was added to the flask. The reaction mixture was cooled to ca. 0 °C using an ice bath. Then, 30 wt% NaOH aq. was dropwise added to the solution over a period of 7 min under cooling. The reaction mixture was allowed to warm up to room temperature without removing the cooling bath. After being stirred for 2 days, the reaction mixture was quenched by the slow addition of 3 M HCl aq. (100 mL). The mixture was extracted with ethyl acetate (ca. 50 mL × 3). The combined organic layers were washed with H_2O and brine, and dried over anhydrous $MgSO_4$. The mixture was filtered, and the filtrate was evaporated. The residue was purified by flash silica-gel column chromatography using hexane/dichloromethane (98/2, v/v) for 1 CV, followed by a gradient elution from hexane/dichloromethane = 98/2 to 80/20 (v/v) over 10 CV at a flow rate of 80 mL min^{-1} to afford **Qx-5** (231.5 mg, 0.257 mmol, 43%) as a white solid. Spectral data for **Qx-5**: ^{1}H NMR (400 MHz, $CDCl_3$): δ = 8.51 (s, 1H), 4.55 (t, J = 6.8 Hz, 2H), 1.93–1.80 (m, 2H), 1.46–1.21 (m, 71H), 0.88 (t, J = 6.8 Hz, 6H) ppm, assigned based on the ^{1}H-^{1}H COSY spectra. ^{13}C NMR (100 MHz, $CDCl_3$): δ = 158.49 (d, J_{CF} = 2.4 Hz), 150.70 (dd, J_{CF} = 243, 17.2 Hz), 148.18 (dd, J_{CF} = 240, 17.1Hz), 140.62 (d, J_{CF} = 3.6 Hz), 136.30 (d, J_{CF} = 4.3 Hz), 133.24 (d, J_{CF} = 3.8 Hz), 109.76 (dd, J_{CF} = 18.4, 2.4 Hz), 107.64 (dd, J_{CF} = 17.8, 1.8 Hz), 68.36, 37.12, 33.53, 31.95, 30.13, 29.73, 29.68, 29.39, 26.67, 25.63, 22.72, 14.15 ppm, assigned based on the DEPT-135, g-HSQC and g-HMBC spectra. The peak assignments are noted on the NMR spectra on pages S34–39. ^{19}F NMR (376 MHz, $CDCl_3$): δ = −118.5 (d, J_{FF} = 24.4 Hz), −123.7 (d, J_{FF} = 24.4 Hz) ppm. MS (MALDI-TOF) m/z = 900.105. FT-IR (ATR) 3058, 2915, 2850, 1881, 1733, 1575, 1470, 1411, 1302, 1226, 1043, 938, 847, 723, 639, 572, 519, 462 cm^{-1}.

Synthesis of Polymer **P1**

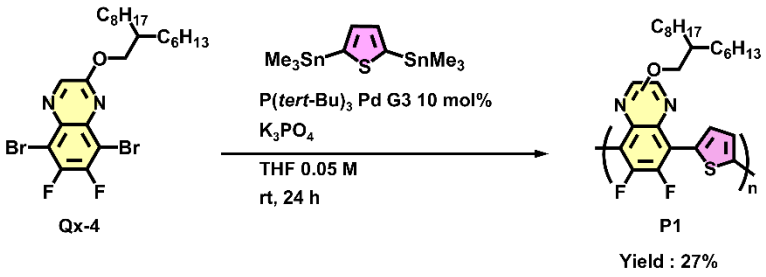

Qx-4 (193.4 mg, 0.343 mmol), 2,5-bis(trimethylstannyl)thiophene (140.8 mg, 0.344 mmol), K_3PO_4 (182.8 mg, 0.861 mmol), and P(*tert*-Bu)$_3$ Pd G3 (19.9 mg, 0.0348 mmol) were added to a 30 mL two-necked flask, which was dried by heating under a reduced pressure in advance. The atmosphere in the flask was replaced with Ar. THF (7.0 mL) was added to the flask. Then, the reaction mixture was stirred at room temperature. The photographs show the color change of the polymerization mixture during the synthesis of **P1**. After being stirred for 24 h, diethylammonium diethyldithiocarbamate (152.4 mg, 0.685 mmol) and chloroform (8.0 mL) were added to the reaction mixture, and the resulting mixture was stirred at room temperature for an additional 1.5 h. Subsequently, the reaction mixture was poured into methanol (200 mL). The precipitate was collected by filtration and purified with Soxhlet extraction using methanol, acetone, hexane, and dichloromethane. The dichloromethane soluble fraction was concentrated and reprecipitated into methanol, yielding **P1** (45.7 mg, 0.0939 mmol, 27%) as a black solid. The chemical structure of **P1** was confirmed by ^{1}H NMR, MALDI-TOF MS, and FT-IR (pages S39, S43, and S46). Spectral data for **P1**: FT-IR (ATR) 2923, 2855, 2728, 2673, 2620, 1578, 1462, 1404, 1313, 1264, 1213, 1092, 1024, 961, 897, 862, 802, 740, 662, 629 cm^{-1}.

Polymerization behavior of **P1**

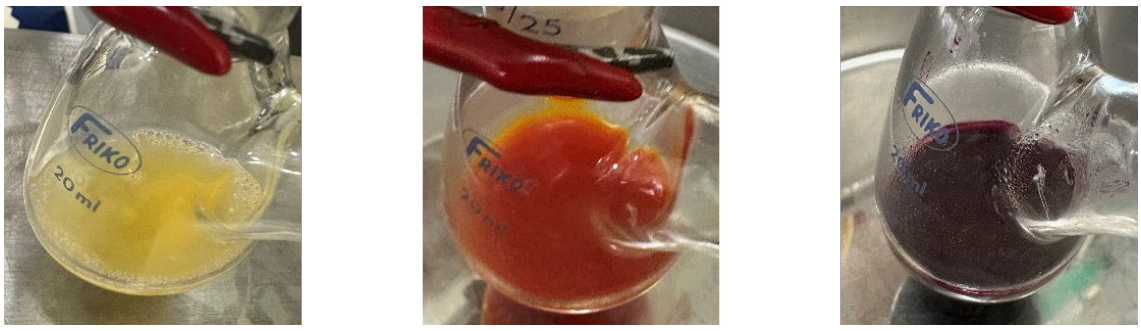

At the start of polymerization	After 6 min	After 13 h
pale yellow	orange	reddish purple

Synthesis of Polymer **P2**

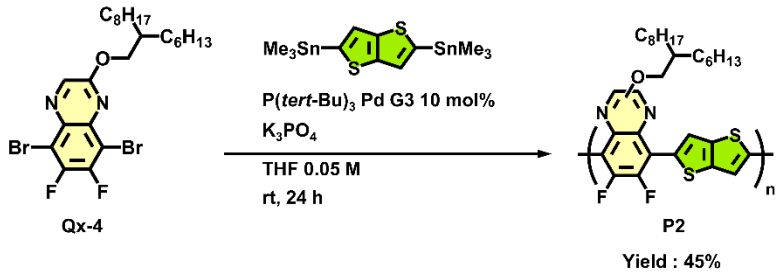

Qx-4 (223.2 mg, 0.395 mmol), 2,5-bis(trimethylstannyl)thieno[3,2-*b*]thiophene (140.8 mg, 0.396 mmol), K_3PO_4 (209.7 mg, 0.988 mmol), and P(*tert*-Bu)$_3$ Pd G3 (23.0 mg, 0.0402 mmol) were added to a 30 mL two-necked flask, which was dried by heating under a reduced pressure in advance. The subsequent polymerization and purification procedures were carried out following the same protocol as that used for **P1**. The photographs show the color change of the polymerization mixture during the synthesis of **P2**. After Soxhlet extraction, the fraction obtained with chloroform following dichloromethane extraction was collected to afford **P2** (97.2 mg, 0.179 mmol, 45%) as black solids. The chemical structure of **P2** was confirmed by ^{1}H NMR, MALDI-TOF MS, and FT-IR (pages S40, S43, and S46). Spectral data for **P2**: FT-IR (ATR) 3136, 3072, 2919, 2854, 2636, 1740, 1641, 1577, 1463, 1404, 1312, 1259, 1211, 1155, 1056, 999, 958, 904, 822, 769, 719, 664 cm^{-1}.

Polymerization behavior of **P2**

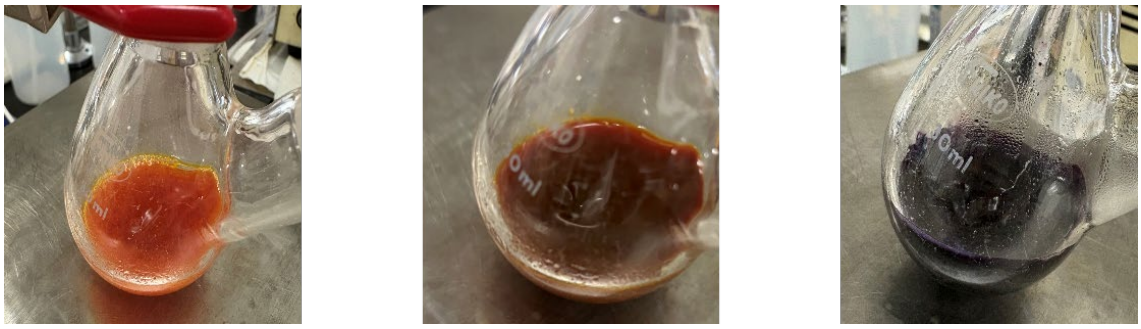

After 6 min	After 2 min	After 35 min
orange	reddish brown	bluish purple

Synthesis of Polymer **P3**

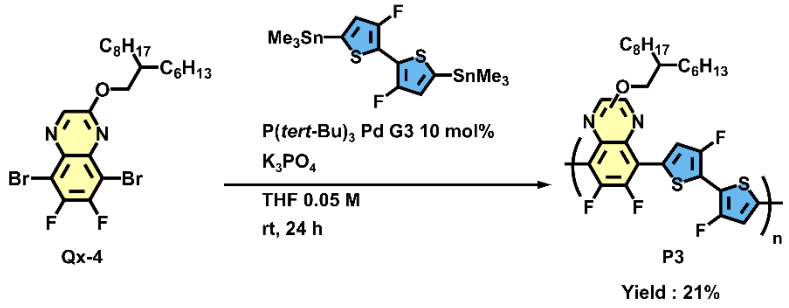

Qx-4 (136.9 mg, 0.243 mmol), (3,3'-difluoro-[2,2'-bithiophene]-5,5'-diyl)bis(trimethylstannane) (128.1 mg, 0.243 mmol), K_3PO_4 (129.3 mg, 0.609 mmol), and P(*tert*-Bu)$_3$ Pd G3 (14.2 mg, 0.0248 mmol) were added to a 20 mL two-necked flask, which was dried by heating under a reduced pressure in advance. The subsequent polymerization and purification procedures were carried out following the same protocol as that used for **P1**. The photographs show the color change of the polymerization mixture during the synthesis of **P3**. After Soxhlet extraction, the fraction obtained with chloroform following dichloromethane extraction was collected to afford **P3** (31.2 mg, 0.0516 mmol, 21%) as black solids. The chemical structure of **P3** was confirmed by ^{1}H NMR, MALDI-TOF MS, and FT-IR (pages S40, S44, and S46). Spectral data for **P3**: FT-IR (ATR) 2968, 2902, 1631, 1574, 1517, 1469, 1417, 1369, 1313, 1270, 1207, 1141, 1071, 1011, 923, 823, 751, 726 cm^{-1}.

Polymerization behavior of **P3**

After 1 min	After 8 min	After 10 h 30 min
orange	reddish brown	bluish purple

Synthesis of Polymer **P4**

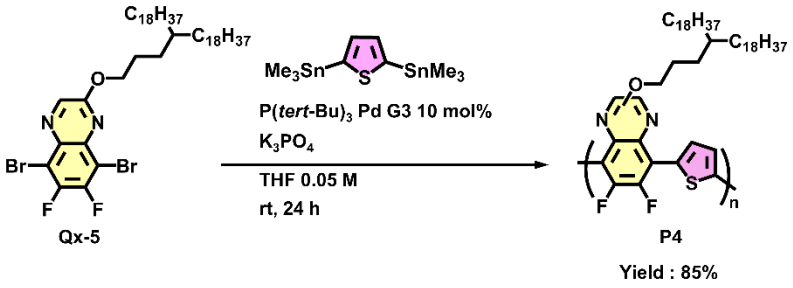

Qx-5 (100.2 mg, 0.111 mmol), 2,5-bis(trimethylstannyl)thiophene (46.0 mg, 0.112 mmol), K_3PO_4 (59.8 mg, 0.282 mmol), and P(*tert*-Bu)$_3$ Pd G3 (19.9 mg, 0.0126 mmol) were added to a 20 mL two-necked flask, which was dried by heating under a reduced pressure in advance. The subsequent polymerization and purification procedures were carried out following the same protocol as that used for **P1**. The photographs show the color change of the polymerization mixture during the synthesis of **P4**. After Soxhlet extraction with methanol followed by acetone, the hexane-extracted fraction was collected to afford **P4** (77.9 mg, 0.0946 mmol, 85%) as a black solid. The chemical structure of **P4** was confirmed by ^{1}H NMR, MALDI-TOF MS, and FT-IR (pages S41, S44, and S46). Spectral data for **P4**: FT-IR (ATR) 2918, 2852, 1580, 1523, 1467, 1419, 1367, 1319, 1263, 1220, 1157, 1091, 1021, 960, 873, 773, 701, 675 cm^{-1}.

Polymerization behavior of **P4**

At the start of polymerization
yellow

After 4 min
reddish brown

After 24 h
bluish purple

Synthesis of Polymer **P5**

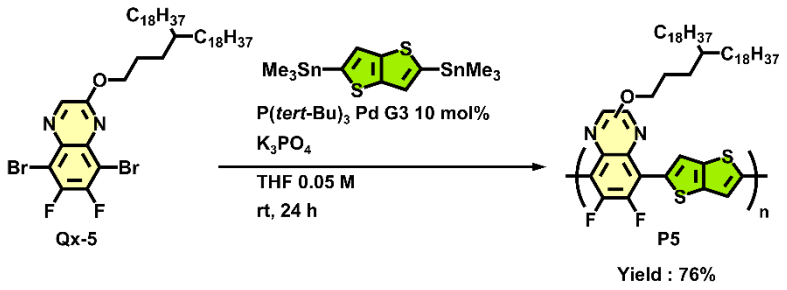

Qx-5 (150.0 mg, 0.166 mmol), 2,5-bis(trimethylstannyl)thieno[3,2-*b*]thiophene (77.6 mg, 0.166 mmol), K_3PO_4 (88.4 mg, 0.417 mmol), and P(*tert*-Bu)$_3$ Pd G3 (9.59 mg, 0.0168 mmol) were added to a 20 mL two-necked flask, which was dried by heating under a reduced pressure in advance. The subsequent polymerization and purification procedures were carried out following the same protocol as that used for **P1**. The photographs show the color change of the polymerization mixture during the synthesis of **P5**. After Soxhlet extraction with methanol followed by acetone, the hexane-extracted fraction was collected to afford **P5** (112 mg, 0.127 mmol, 76%) as a black solid. The chemical structure of **P5** was confirmed by ^{1}H NMR, MALDI-TOF MS, and FT-IR (pages S41, S45, and S46). Spectral data for **P5**: FT-IR (ATR) 2918, 2851, 2669, 1638, 1580, 1466, 1408, 1317, 1257, 1211, 1080, 1034, 969, 903, 813, 721, 663, 622 cm^{-1}.

Polymerization behavior of **P5**

After 6 min
reddish brown

After 15 min
reddish purple

After 1 h 15 min
bluish purple

Synthesis of Polymer **P6**

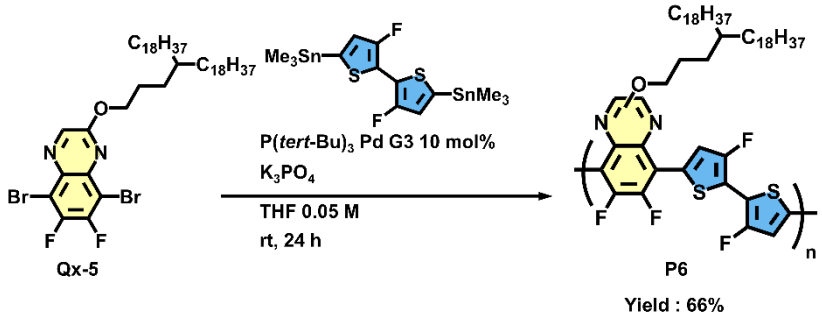

Qx-5 (150.1 mg, 0.166 mmol), (3,3'-difluoro-[2,2'-bithiophene]-5,5'-diyl)bis(trimethylstannane) (87.9 mg, 0.167 mmol), K_3PO_4 (89.2 mg, 0.420 mmol), and P(*tert*-Bu)$_3$ Pd G3 (9.77 mg, 0.0171 mmol) were added to a 20 mL two-necked flask, which was dried by heating under a reduced pressure in advance. The subsequent polymerization and purification procedures were carried out following the same protocol as that used for **P1**. The photographs show the color change of the polymerization mixture during the synthesis of **P6**. After Soxhlet extraction with methanol followed by acetone, the hexane-extracted fraction was collected to afford **P6** (104 mg, 0.110 mmol, 66%) as a black solid. The chemical structure of **P6** was confirmed by ^{1}H NMR, MALDI-TOF MS, and FT-IR (pages S42, S45, and S46). Spectral data for **P6**: FT-IR (ATR) 2917, 2851, 1580, 1463, 1407, 1317, 1273, 1219, 1152, 1091, 1037, 959, 904, 856, 771, 677, 624 cm^{-1}.

Polymerization behavior of **P6**

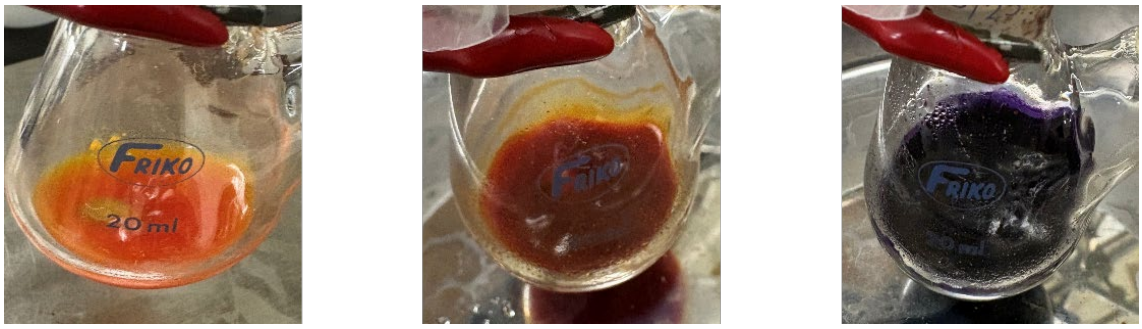

After 1 min	After 5 min	After 9 h 15 min
orange	reddish brown	bluish purple

3. Fig. S1–S24

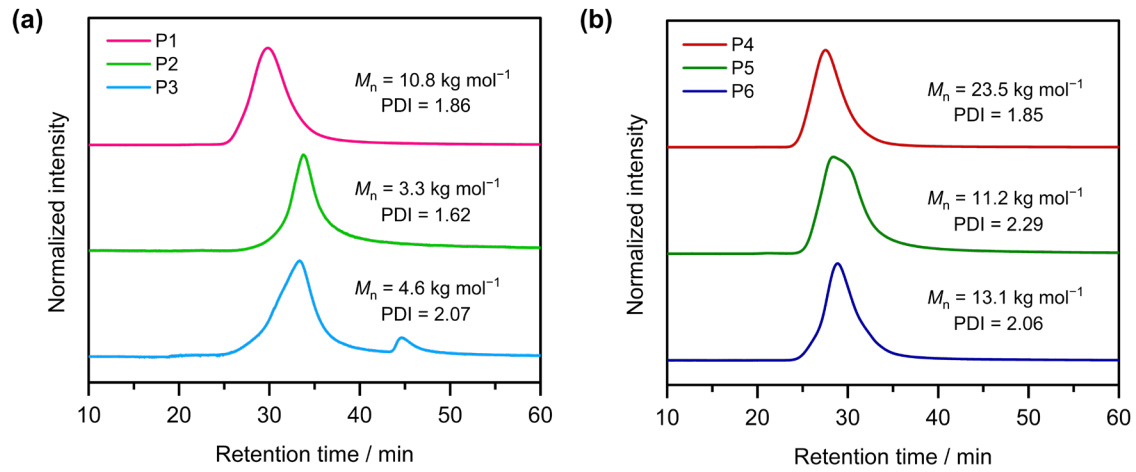

Fig. S1 GPC traces of the synthesized polymers measured in *o*-DCB at 40 °C. (a) **P1**–**P3**. (b) **P4**–**P6**.

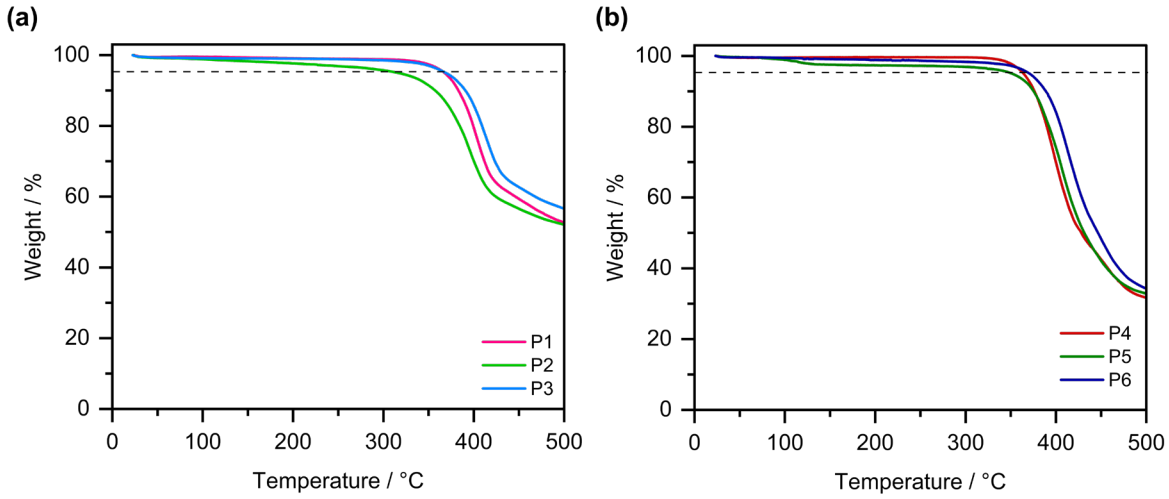

Fig. S2 TGA curves of (a) **P1**–**P3** and (b) **P4–P6** recorded under nitrogen atmosphere at a rate of 10 °C min^{-1}.

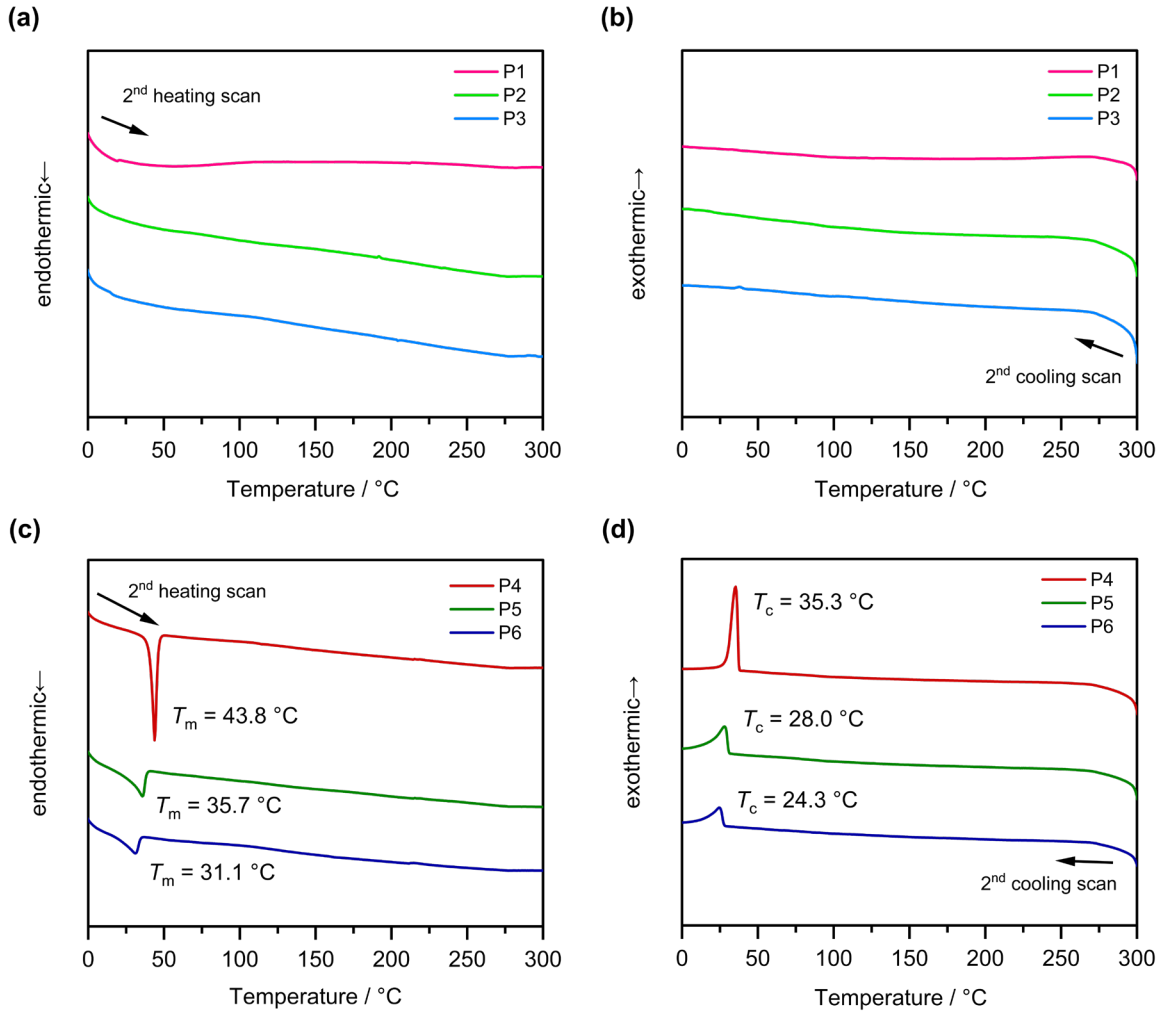

Fig. S3 DSC thermograms of **P1**–**P6** measured under nitrogen atmosphere at a rate of 10 °C min^{-1}. Second (a) heating and (b) cooling scans of **P1**–**P3**. Second (c) heating and (d) cooling scans of **P4–P6**.

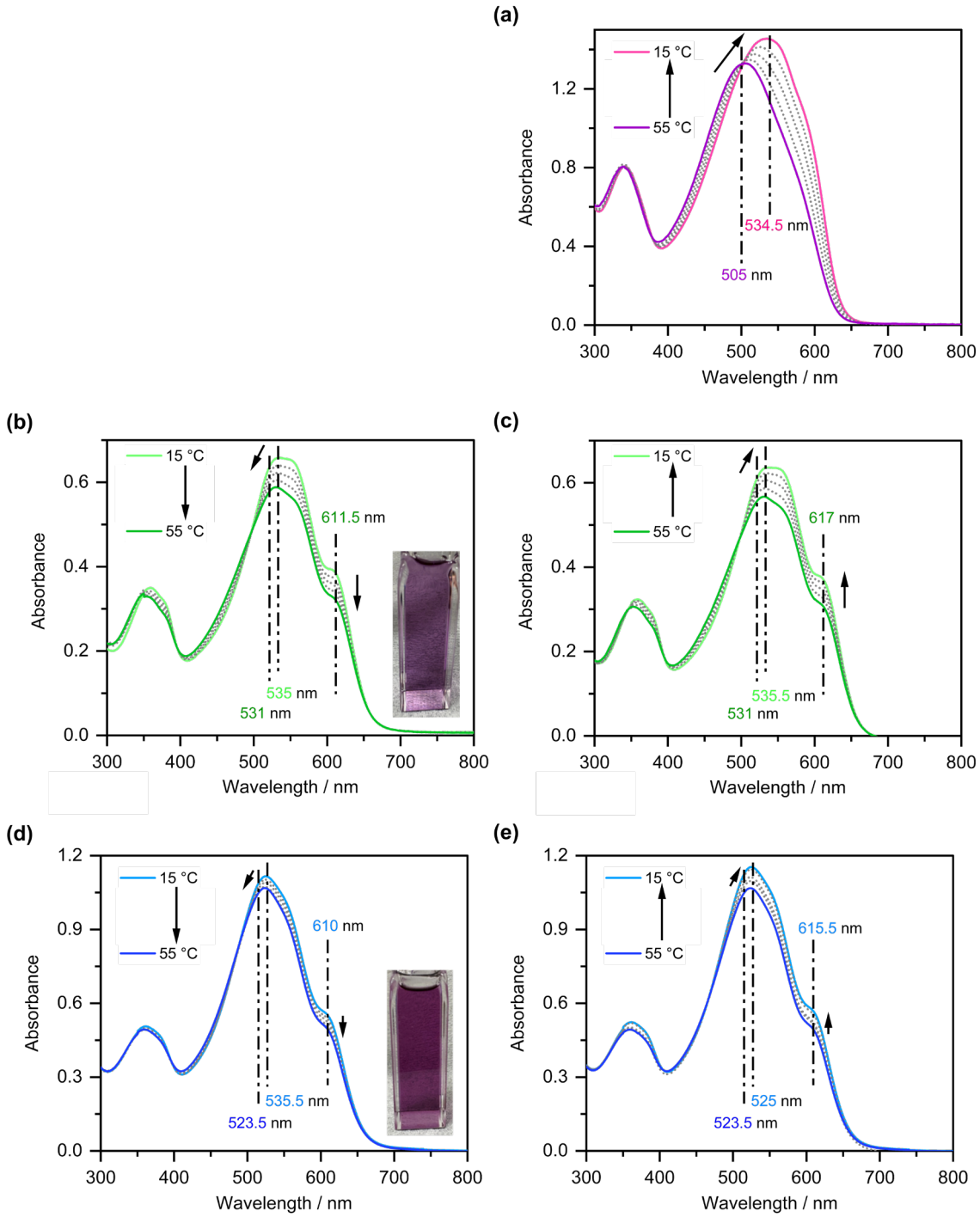

Fig. S4 Temperature-dependent UV–vis absorption spectra of **P1–P3** dissolved in chloroform (c = ca. 1.0 × 10^{-5} M): (a) cooling process of **P1**; (b) heating and (c) cooling processes of **P2**; (d) heating and (e) cooling processes of **P3**. All spectra were recorded between 15 and 55 °C at 10 °C intervals.

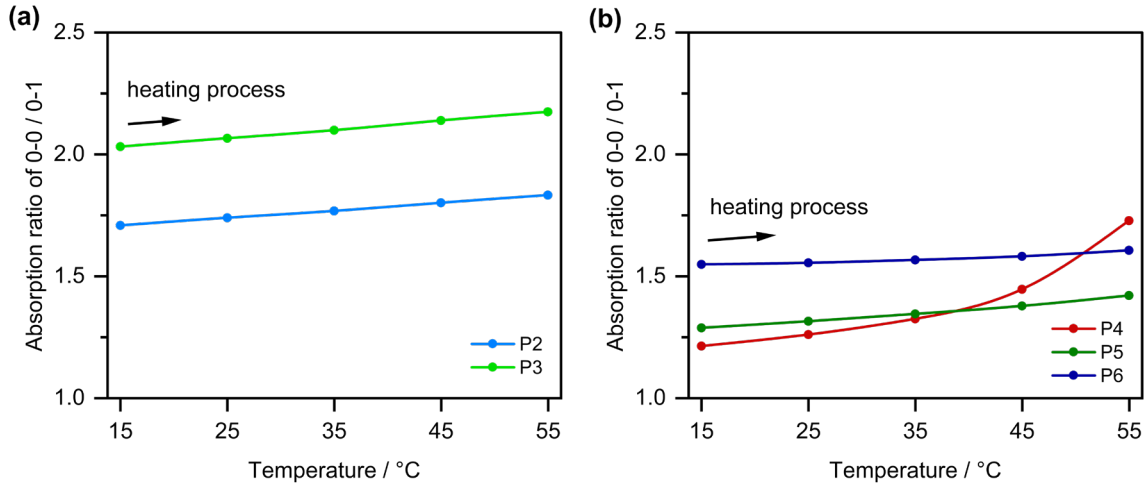

Fig. S5 Absorption ratios of 0–0/0–1 peaks of (a) **P2–P3** and (b) **P4–P6** dissolved in $CHCl_3$ (c = ca. 1.0 × 10^{-5} M) obtained by heating from 15 to 55 °C.

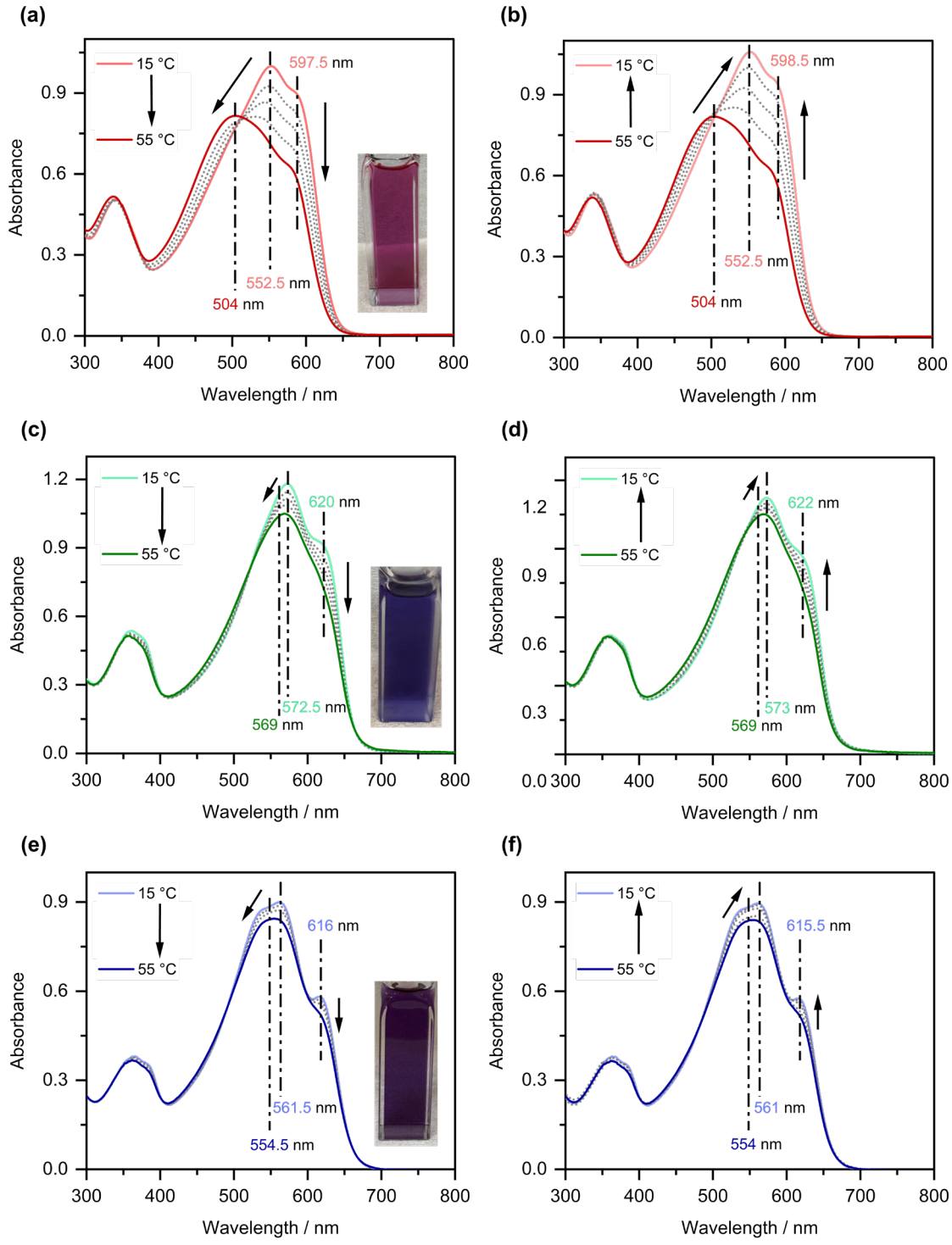

Fig. S6 Temperature-dependent UV–vis absorption spectra of **P4–P6** dissolved in chloroform (c = ca. 1.0 × 10^{-5} M): (a) heating and (b) cooling processes of **P4**; (c) heating and (d) cooling processes of **P5**; (d) heating and (e) cooling processes of **P6**. All spectra were recorded between 15 and 55 °C at 10 °C intervals.

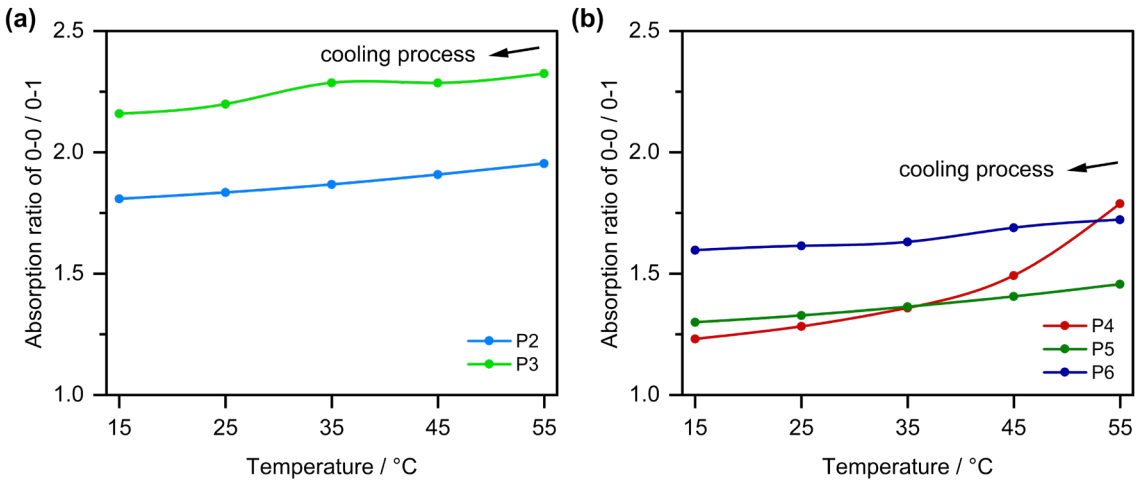

Fig. S7 Absorption ratios of 0–0/0–1 peaks of (a) **P2–P3** and (b) **P4–P6** dissolved in $CHCl_3$ (c = 1.0 × 10^{-5} M) obtained by cooling from 55 to 15 °C.

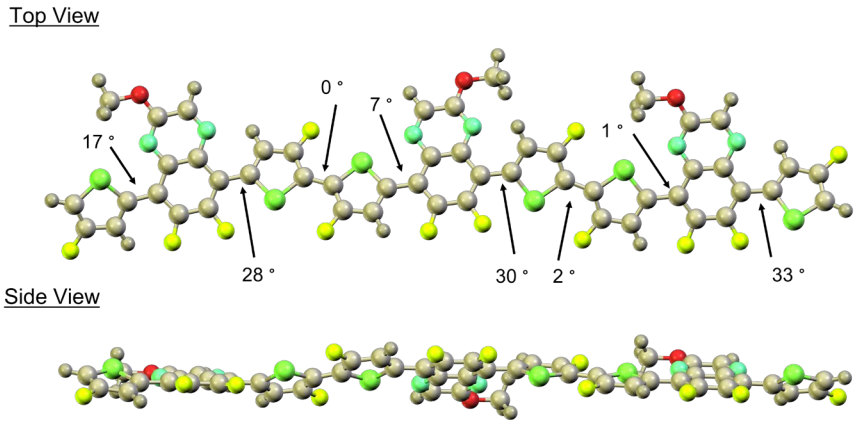

Fig. S8 Optimized geometries and conformational analysis of **P3** and **P6** models calculated at the ωB97XD/6-31G(d,p) level, where the alkyl side chains were replaced with methyl groups.

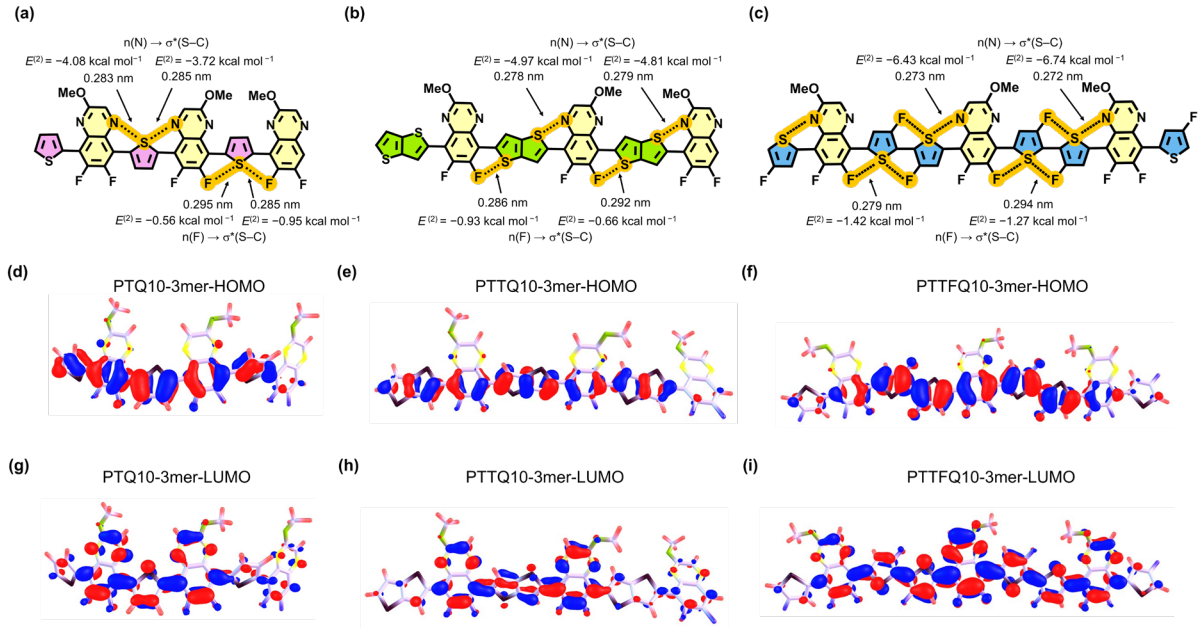

Fig. S9 Optimized molecular geometries, NBO analyses, and frontier molecular orbitals of (a,d,g) **P1** and **P4**, (b, e, h) **P2** and **P5**, and (c, f, i) **P3** and **P6** model compounds. (a–c) NBO analyses highlighting S–F and S–N noncovalent interactions, including the corresponding interatomic distances and second-order perturbation stabilization energies ($E^{(2)}$). The HOMO (d–f) and LUMO (g–i) distributions along the conjugated backbone are shown. All calculations were performed at the ωB97XD/6-31G(d,p) level of theory.

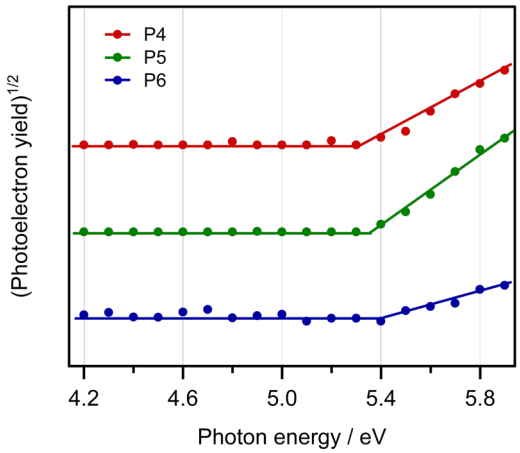

Fig. S10 Photoelectron yield spectroscopy (PYS) spectra of thin films of **P4**–**P6** prepared on OTMS-modified SiO_2 (300 nm)/Si substrates. The HOMO levels were determined from the onset of photoelectron emission.

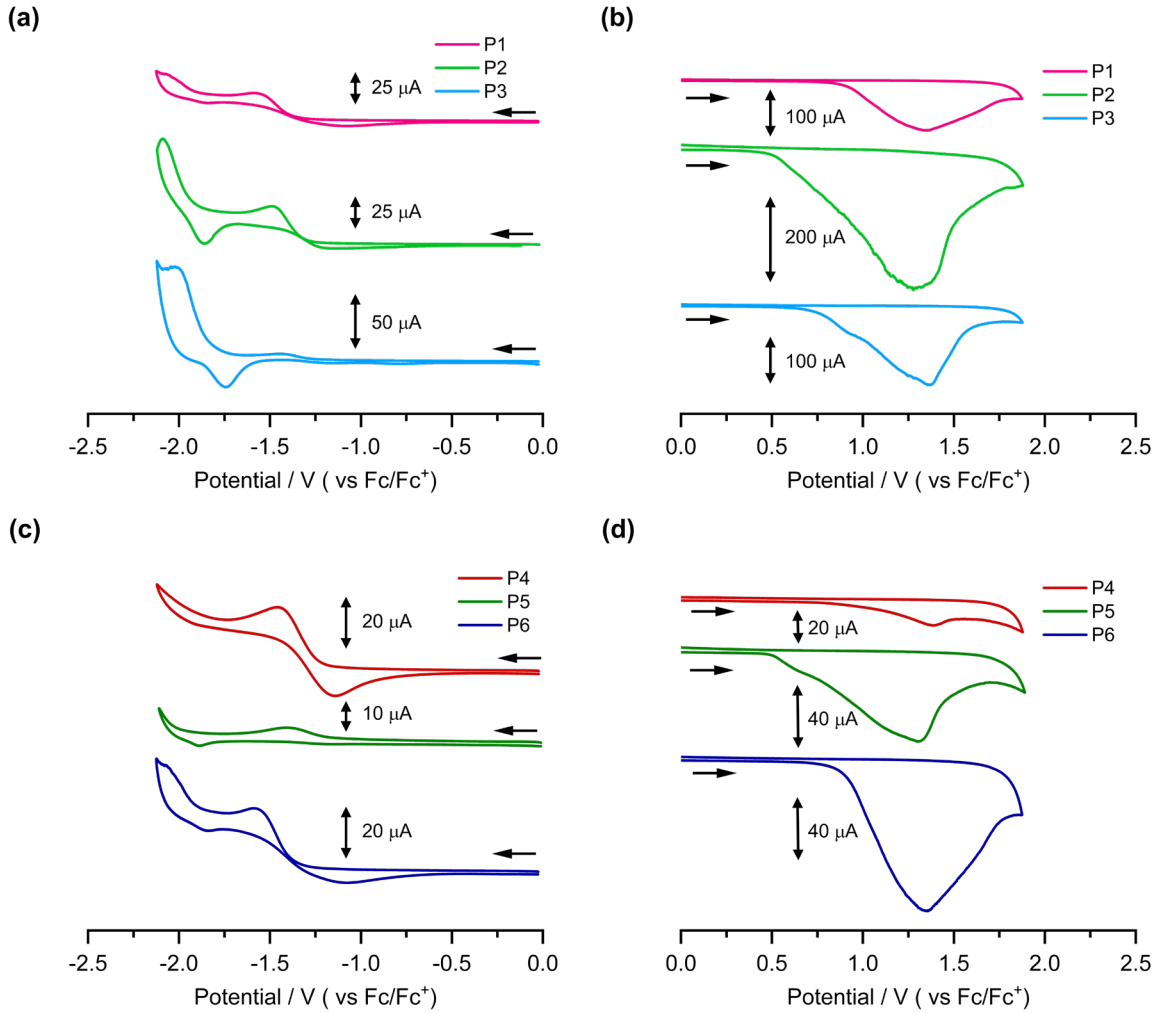

Fig. S11 Cyclic voltammograms of polymer thin films, measured in MeCN with 0.1 M *n*-Bu_4NClO_4 at a scan rate of 100 mV s^{-1}: (a) reduction of **P1–P3**, (b) oxidation of **P1–P3**, (c) reduction of **P4–P6**, and (d) oxidation of **P4–P6**.

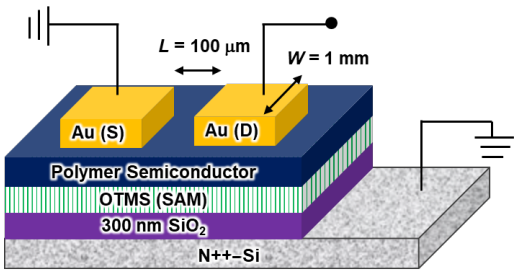

Fig. S12 Schematic illustration of the top-contact/ bottom-gate (TC/BG) organic field-effect transistor (OFET) device architecture used in this study.

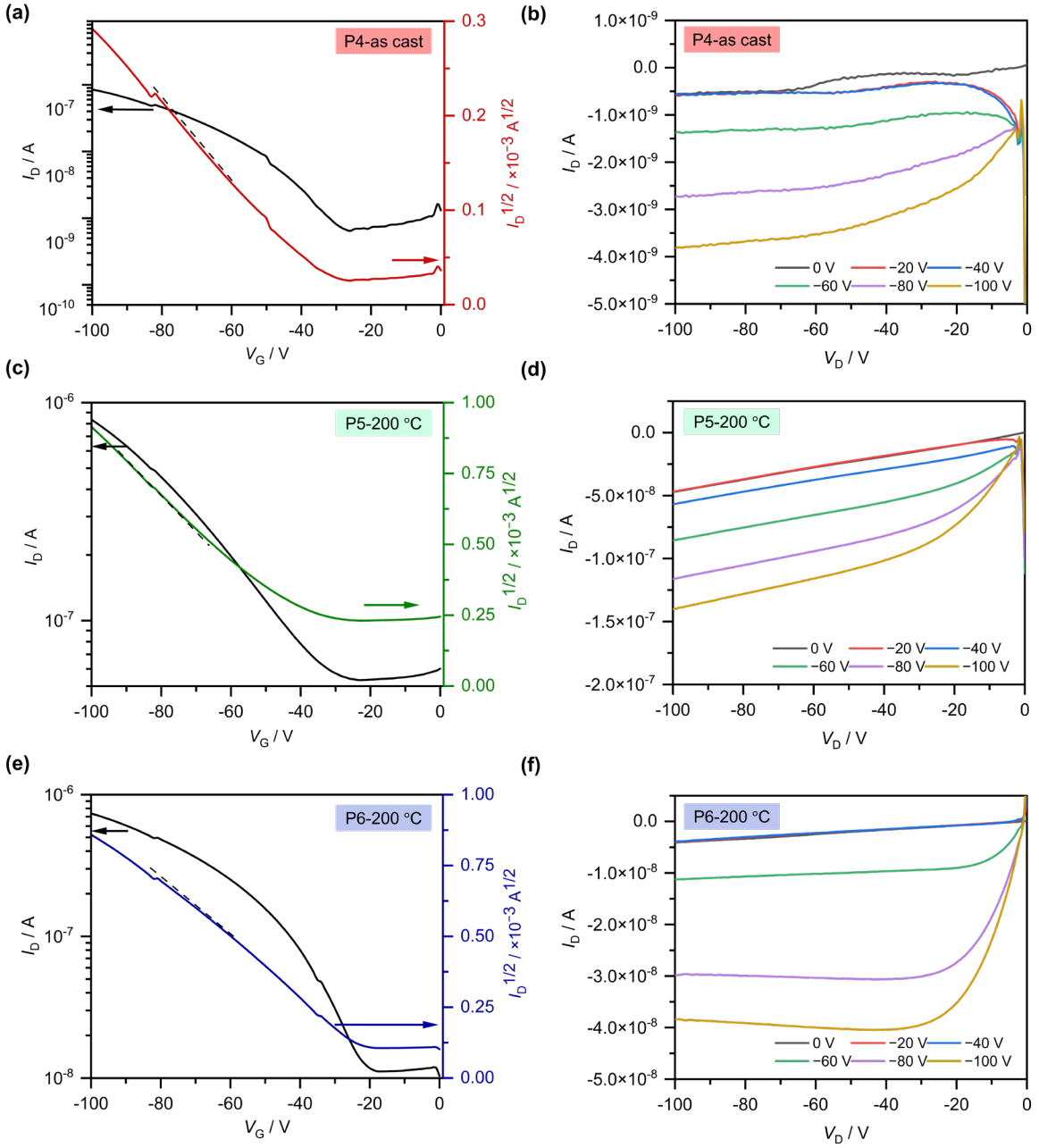

Fig. S13 Transfer curves of OFET devices based on (a) **P4** (as-cast), (c) **P5** after thermal annealing at 200 °C, and (e) **P6** after thermal annealing at 200 °C. Panels (a, c, e) show the transfer curves ($V_D = -100$ V) measured in air, while panels (b, d, f) show the corresponding output curves. The drain current (I_D) –drain voltage (V_D) curves were measured at different gate voltages (V_G).

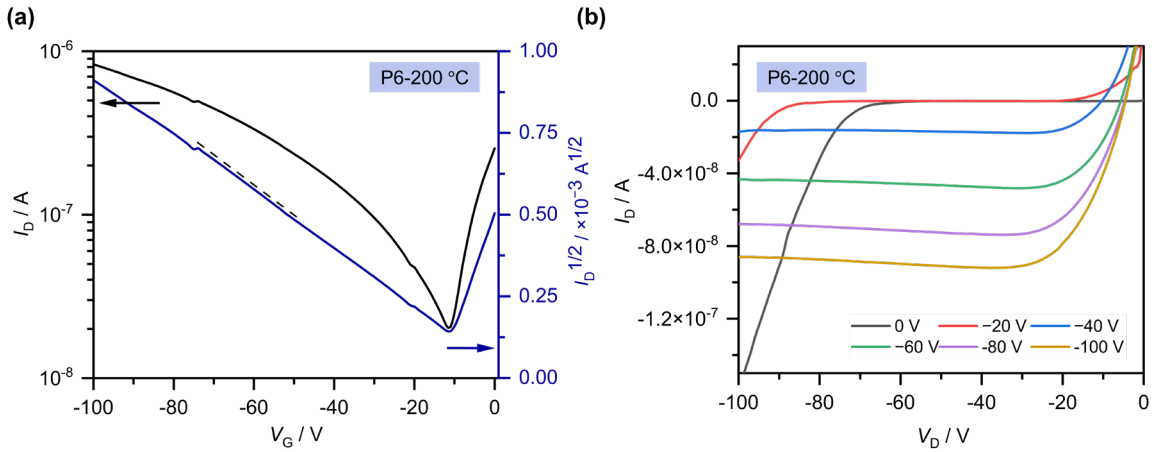

Fig. S14 (a) Transfer (V_D = −100 V) and (b) the corresponding output curves of OFET devices based on **P6** after thermal annealing at 200 °C, measured under vacuum. The drain current (I_D) –drain voltage (V_D) curves were measured at different gate voltages (V_G).

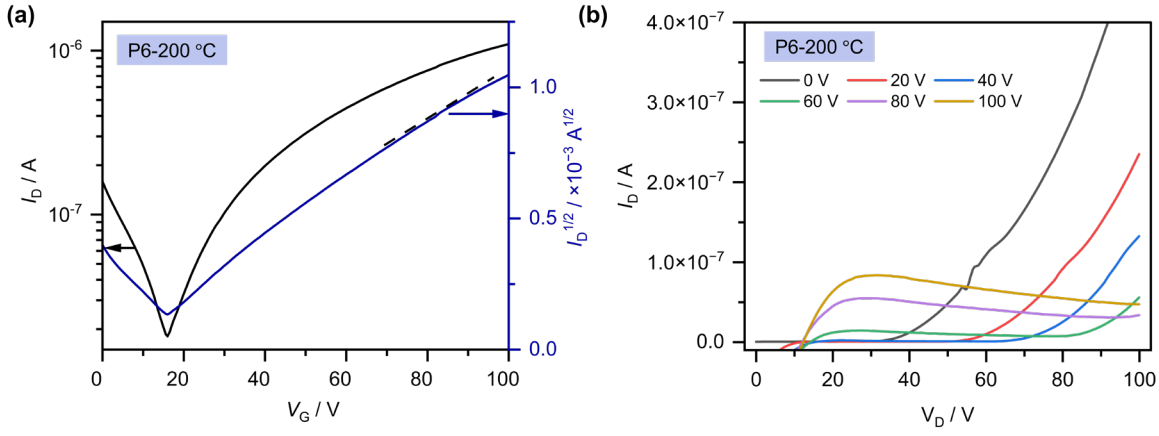

Fig. S15 (a) Transfer (V_D = 100 V) and (b) the corresponding output curves of OFET devices based on **P6** after thermal annealing at 200 °C, measured under vacuum. The drain current (I_D) –drain voltage (V_D) curves were measured at different gate voltages (V_G).

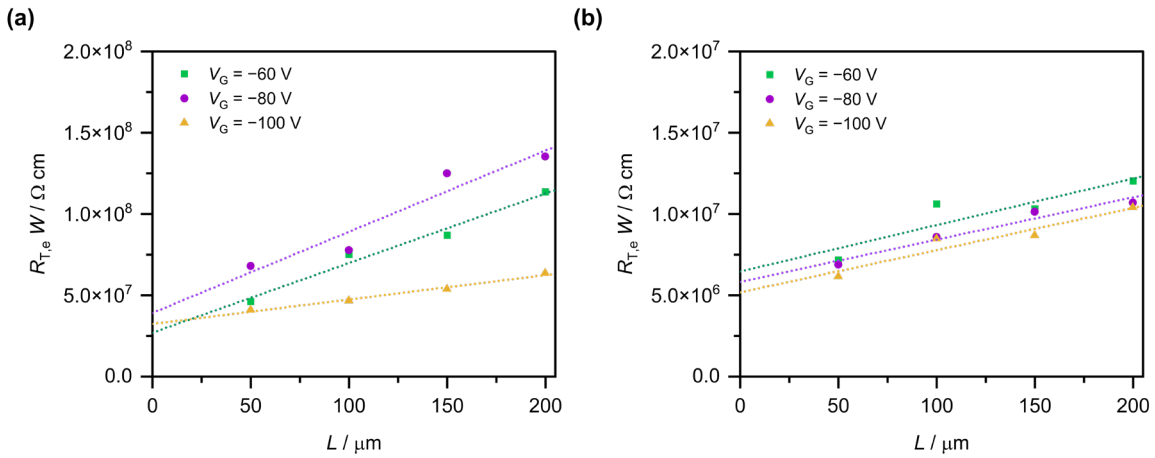

Fig. S16 Width-normalized total resistance ($R_{T,e}W$) as a function of channel length for **P6** OFET devices with Au contacts measured under vacuum conditions: (a) p-type operation and (b) n-type operation. Linear fitting based on the transmission line method (TLM) was used to extract contact and channel resistance components.

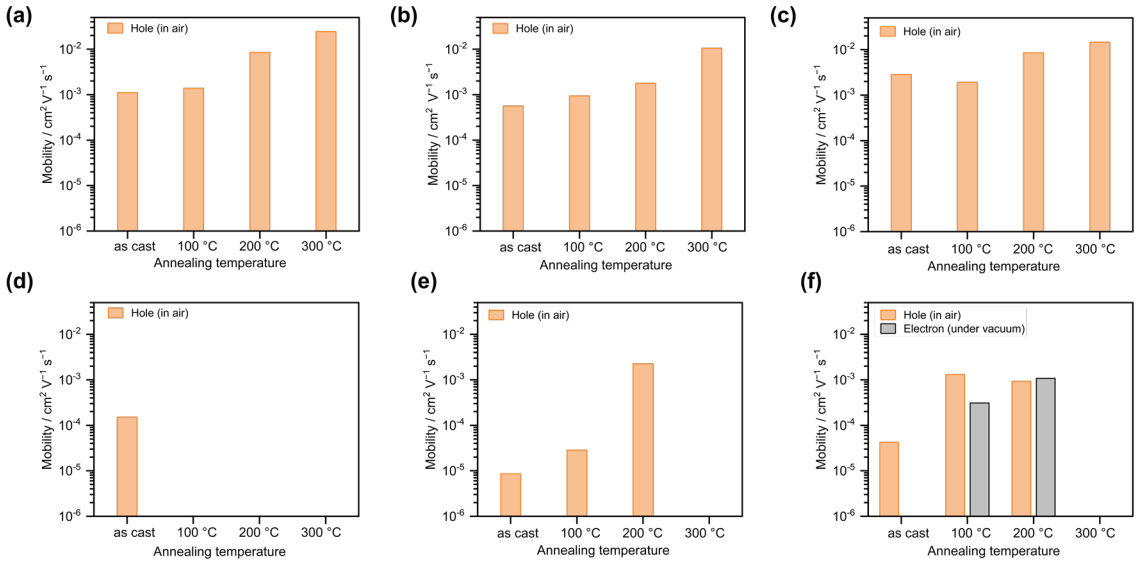

Fig. S17 Average hole mobility values of OFET devices based on **P1**–**P6**, calculated from five independent devices, as a function of annealing temperature: (a) **P1**, (b) **P2**, (c) **P3**, (d) **P4**, (e) **P5**, and (f) **P6**. The absence of a bar indicates that the devices did not function at the corresponding annealing temperature.

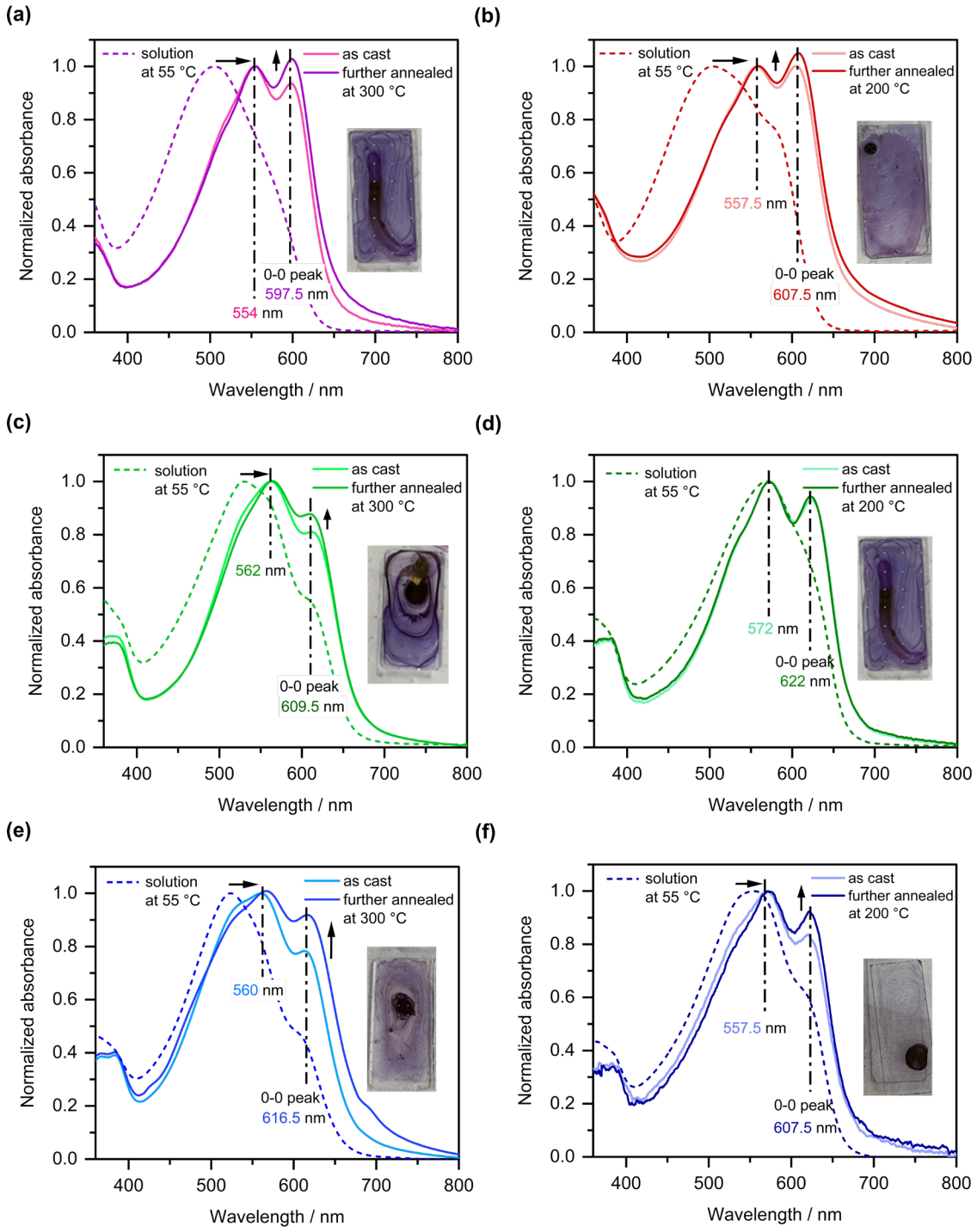

Fig. S18 Normalized UV–vis absorption spectra of **P1**–**P6**. The spectra of partially dispersed polymer solutions in chloroform at 55 °C are shown as dashed lines, while the absorption spectra of thin films in the as-cast state and after thermal annealing are shown as solid lines. **P1–P3** were annealed at 300 °C and **P4–P6** were annealed at 200 °C, respectively: (a) **P1**, (b) **P4**, (c) **P2**, (d) **P5**, (e) **P3**, and (f) **P6**.

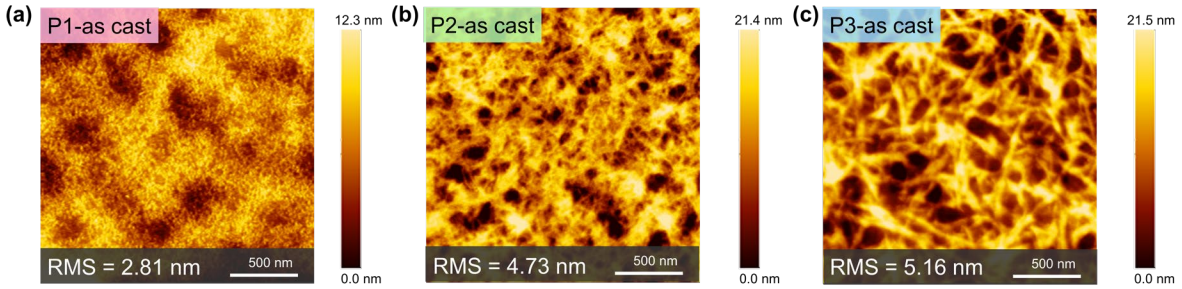

Fig. S19 AFM height images (2 × 2 μm^2) of the as-cast thin films of (a) **P1**, (b) **P2**, and (c) **P3**. The root-mean-square (RMS) roughness values are indicated in the respective panels.

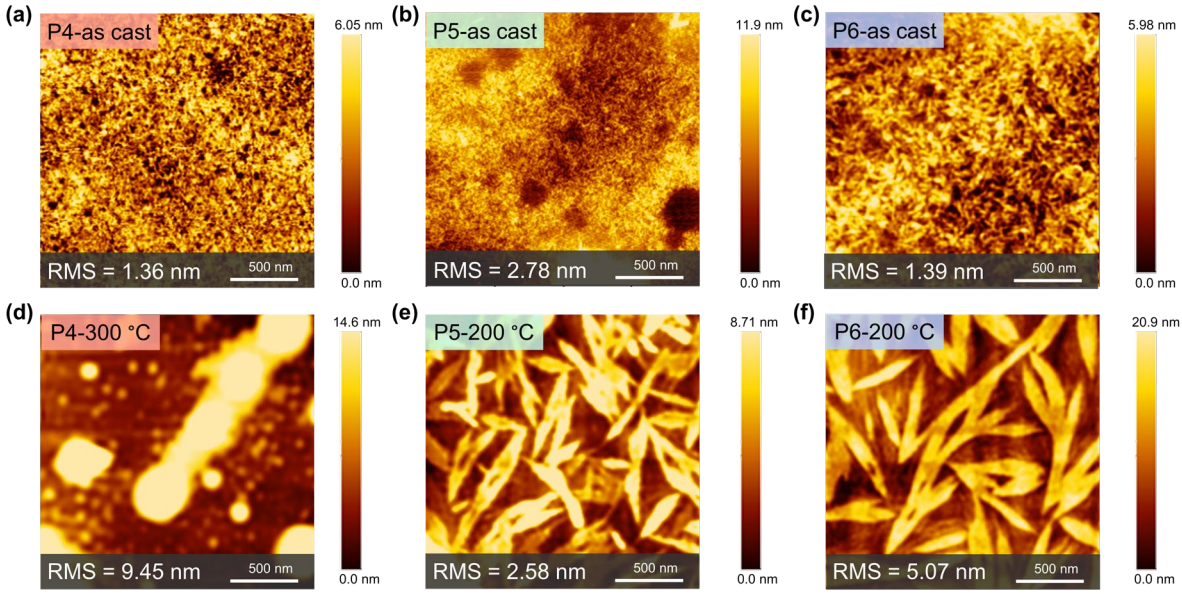

Fig. S20 AFM height images (2 × 2 μm^2) of **P4–P6** thin films before and after thermal annealing: (a) As-cast **P4**, (b) as-cast **P5**, (c) as-cast **P6**, (d) **P4** annealed at 300 °C, (e) **P5** annealed at 200 °C, and (f) **P6** annealed at 200°C. The RMS roughness values are indicated in the respective panels.

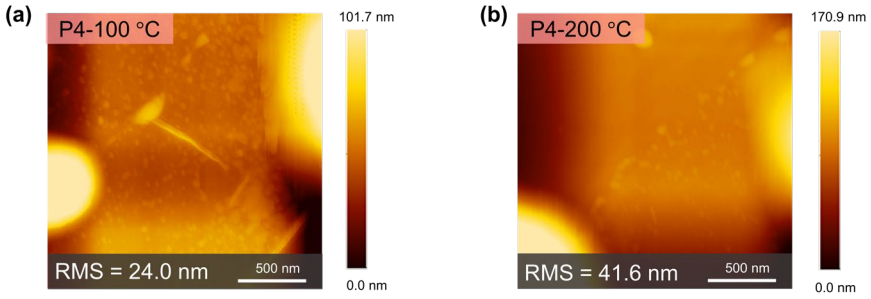

Fig. S21 AFM height images (2 × 2 μm^2) of **P4** thin films after thermal annealing: (a) **P4** annealed at 100 °C, and (b) **P4** annealed at 200°C. The RMS roughness values are indicated in the respective panels.

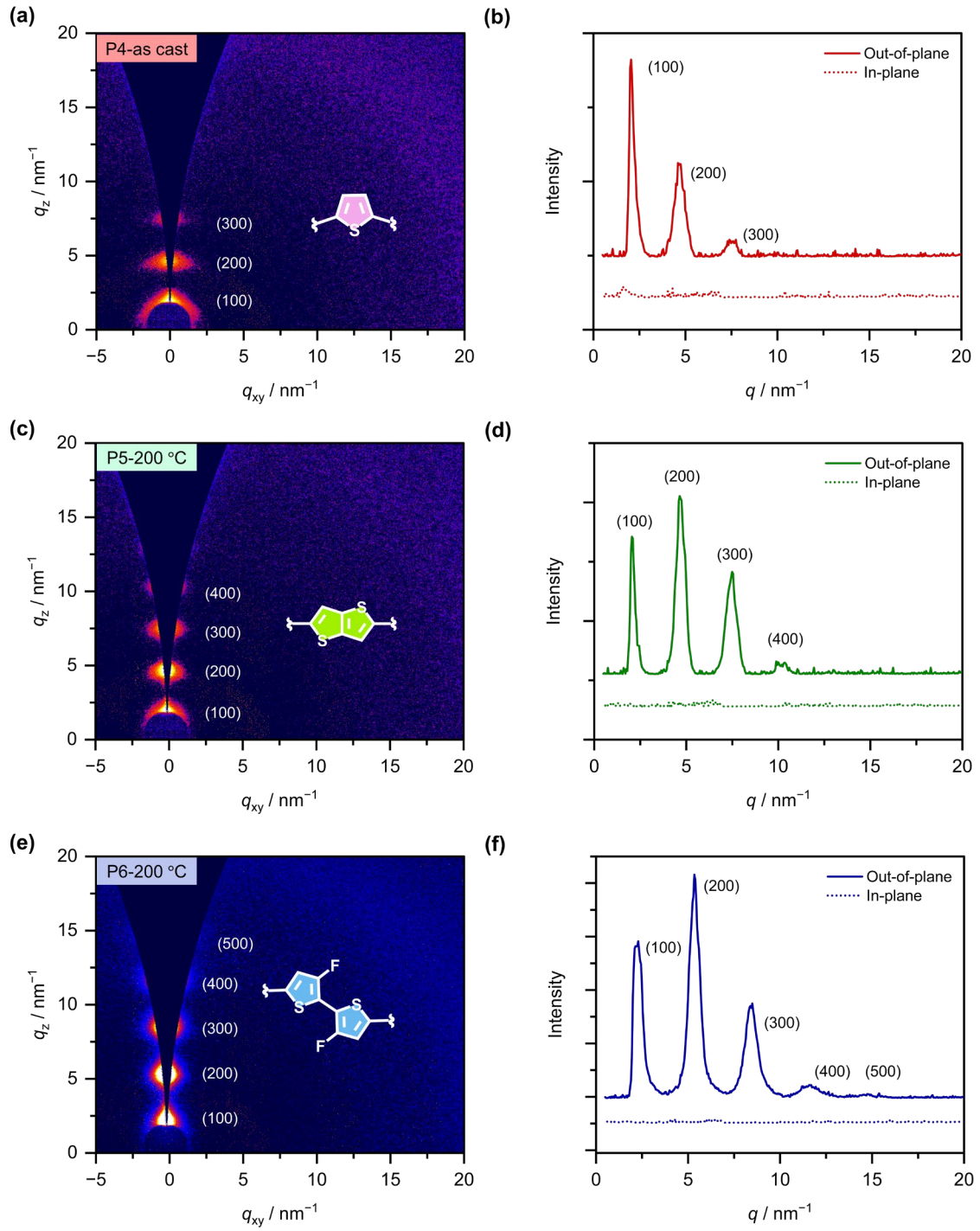

Fig. S22 GIWAXS characterization of polymer thin films. (a, c, e) 2D GIWAXS images of (a) **P4** (as cast), (c) **P5** (annealed at 200 °C), and (e) **P6** (annealed at 200 °C). (b, d, f) 1D Line-cut profiles, extracted from the out-of-plane (q_z, solid lines) and in-plane (q_{xy}, dotted lines) directions, of (b) **P4** (as cast), (d) **P5** (annealed at 200 °C), and (f) **P6** (annealed at 200 °C).

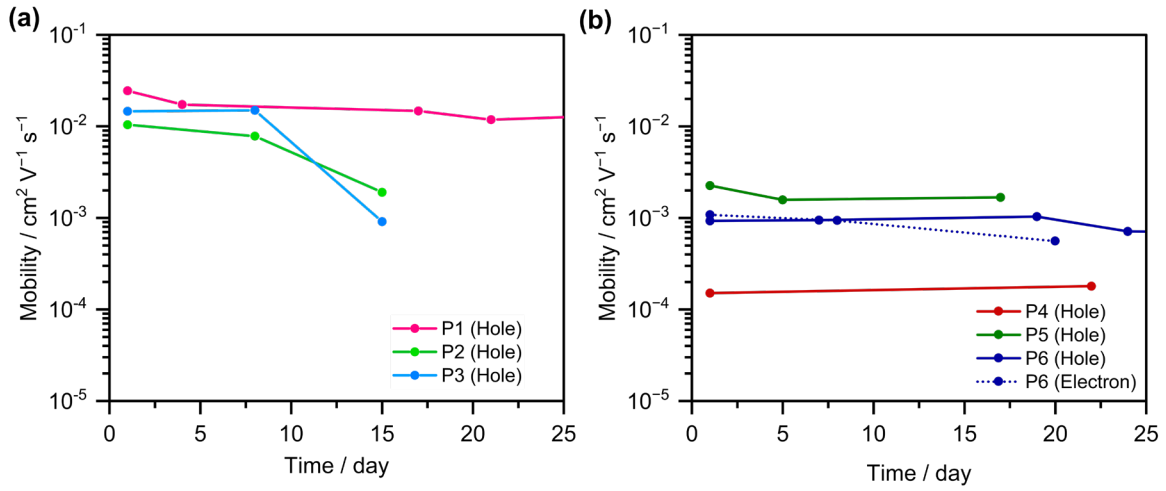

Fig. S23 Stability of field-effect mobility for (a) short-branched (**P1–P3**) and (b) long-branched (**P4–P6**) polymers as a function of storage time in a nitrogen-filled glovebox. All p-type mobilities were measured in air, and n-type mobility for **P6** was measured under vacuum.

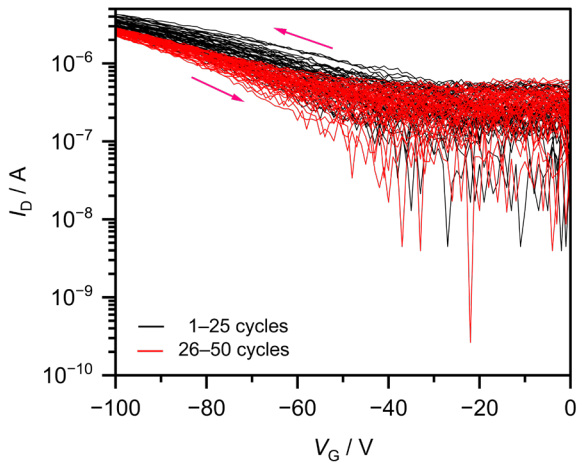

Fig. S24 Transfer characteristics (I_D–V_G, V_D = −100 V) of the OFET device based on **P1** measured over 50 consecutive cycles in air. The curves corresponding to cycles 1–25 and 26–50 are shown in black and red, respectively.

4. Tables S1−S7

PTQ-based semiconducting polymers

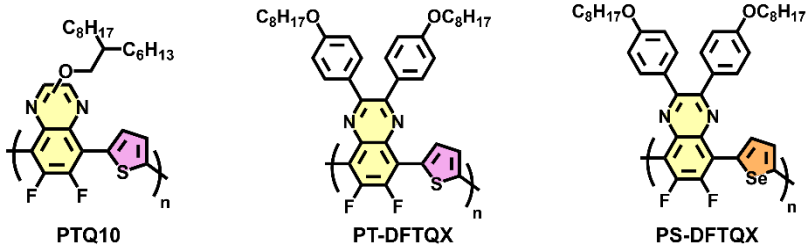

PTQ10 PT-DFTQX PS-DFTQX

Table S1 Comparison of field-effect transistor mobilities in quinoxaline-based semiconducting polymers with reported literatures.

Polymer	Operation mode	μ [a] ($cm^2 V^{-1} s^{-1}$)	Device configuration[b]	Source/Drain electrode	W/L [c]	Reference
P1 (this work)	**p-type**	**2.45×10^{-2}**	**TC/BG**	**50 nm Au**	**10**	**-**
PTQ10	p-type	2.45×10^{-3}	BC/BG	4 nm Cr / 40 nm Au	1000	41
PT-DFTQX	p-type	1.2×10^{-3}	BC	100 nm Au	10	63
PS-DFTQX	p-type	1.7×10^{-2}	BC	100 nm Au	10	63
PQx-TVT	p-type	1.1×10^{-3}	BC /TG	50 nm Au	8	42
PQx-QC	p-type	1.4×10^{-3}	TC/BG	100 nm Au	20	47
PQx-TDPP	n-type	1.22	BC/TG	3 nm Cr / 30 nm Au	50	43
PQx-IDT	p-type	1.1×10^{-1}	BC/BG	50 nm Au	20	46
PNPI2T-*o*F2	p-type	1.4×10^{-1}	BC/ TG	Cr/Au	400	45
PNPI2T-*o*F2	n-type	7.1×10^{-1}	BC/ TG	Cr/Au	400	45

[a] Field-effect mobilities were reported as average values calculated from five independent devices for this work, whereas the literature values were cited as reported.

[b] Device configuration: TC/BG, top-contact/bottom-gate; BC/BG, bottom-contact/bottom-gate; BC/TG, bottom-contact/top-gate.

[c] W and L denote the channel width and length, respectively.

4.1 Polymerization conditions

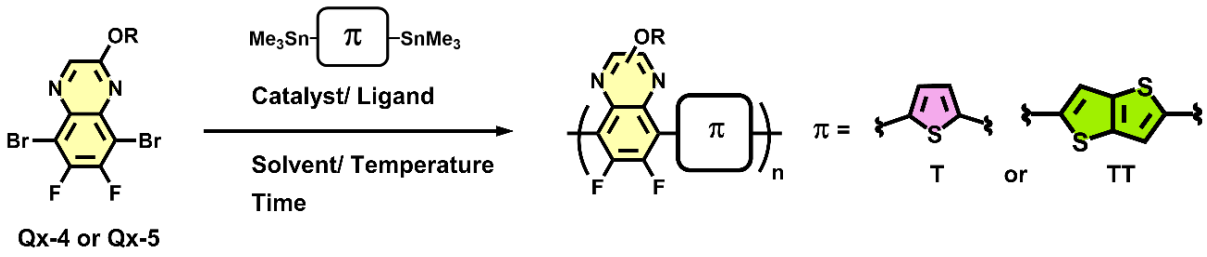

Table S2 Polymerization conditions and the resulting molecular weights of quinoxaline-based semiconducting polymers.

#	Monomer	π	Catalyst/ Ligand	Additive	Solvent /Temperature	Time	M_n[a] (g mol^{-1})	PDI[a]
1	Qx-4	T	P(*tert*-Bu)$_3$ Pd G3 10 mol%	K_3PO_4	THF / rt	24 h	10.8 k	1.86
2	Qx-4	T	Pd_2dba_3 / P(*o*-tolyl)$_3$ 2 mol%/ 8 mol%	-	Toluene / reflux	16 h	2.4 k	1.61
3	Qx-5	T	Pd_2dba_3 / P(*o*-tolyl)$_3$ 4.4 mol%/ 17.6 mol%	CuI	Ph-Cl / reflux	48 h	6.4 k	1.89
4	Qx-5	TT	Pd_2dba_3 / P(*o*-tolyl)$_3$ 4.4 mol%/ 17.6 mol%	CuI	Ph-Cl / reflux	48 h	6.4 k	2.24

[a] Determined by GPC using *o*-DCB as the eluent at 40 °C, calibrated against polystyrene standards.

4.2 Synthetic complexity index

A detailed derivation of the synthetic complexity index (SCI) has been reported in the perspective by Po *et al.*[S7], and additional discussions focusing on conjugated polymer synthesis are described in a previous work [S8]. In this study, normalization was performed using the synthesis of D18, a representative donor polymer in the OPV field, as a reference.[S9]

$$\mathrm{SCI} = 35 \times \frac{N_{SS}}{N_{SS,MAX}} + 25 \times \frac{\log(RY)}{\log(RY_{MAX})} + 15 \times \frac{N_O}{N_{O,MAX}} + 15 \times \frac{N_C}{N_{C,MAX}} + 10 \times \frac{N_H}{N_{H,MAX}}$$

where N_{SS} is the number of synthetic steps (SS), RY is the reciprocal yield of the overall yield, N_O is the number of operations, including purification steps such as quenching, extraction, precipitation, recrystallization, and Soxhlet extraction, N_C is the number of chromatographic purifications, i.e., the number of column chromatography steps, and N_H is the number of associated GHS hazard codes (H-codes) assigned to the chemicals used in the polymerization step. The hazard categories and corresponding codes considered in this study include: carcinogenic/mutagenic (H340, H341, H350, H351), toxic to reproduction (H360, H361), highly toxic (H300, H304, H310, H330, H370, H372), environmentally toxic (H400, H410,

H411), highly reactive with water (H260, H261), highly flammable (H220, H222, H224, H250), highly corrosive (H290, H314, H318), and explosive (H200, H201, H202, H203, H204, H205, H240, H241, H271).

Table S3 Parameters used for the calculation of the polymerization-based SCI for D18 and polymers **P1–P6**.

Polymer	N_{SS}	Yield	RY	N_O	N_C	N_H	SCI
D18	22	2.33%	42.9	26	12	138	100
P1	5	8.78%	11.4	8	1	23	31.7
P2	5	18.9%	5.29	9	1	23	27.1
P3	5	8.85%	11.3	9	1	23	32.2
P4	5	26.1%	3.83	9	1	31	25.6
P5	5	23.3%	4.29	9	1	31	26.3
P6	5	20.3%	4.93	9	1	31	27.3

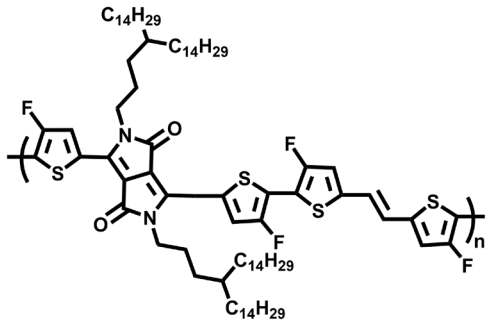

fDT-DPP-based copolymers

Table S4 Parameters used for the calculation of the polymerization-based SCI for fDT-DPP-based copolymers and polymers **P1–P6**.

Polymer	N_{SS}	Yield	RY	N_O	N_C	N_H	SCI
fDT-DPP based	10	1.91%	52.4	20	7	48	100
P1	5	8.78%	11.4	8	1	23	47.7
P2	5	18.9%	5.29	9	1	23	43.7
P3	5	8.85%	11.3	9	1	23	48.4
P4	5	26.1%	3.83	9	1	31	43.4
P5	5	23.3%	4.29	9	1	31	44.0
P6	5	20.3%	4.93	9	1	31	44.9

4.3 Characteristics

Table S5 Electrochemically determined HOMO and LUMO energy levels and the corresponding band gaps (E_{gap}^{CV}) for polymers **P1–P6**.

Polymer	E_{HOMO}^{CV}/ eV	E_{LUMO}^{CV}/ eV	E_{gap}^{CV}/ eV
P1	−5.57	−3.36	2.21
P2	−5.31	−3.45	1.86
P3	−5.54	−3.54	2.00
P4	−5.60	−3.56	2.26
P5	−5.29	−3.63	1.66
P6	−5.68	−3.42	2.26

Table S6 Summary of total resistance ($R_{T,e}$), contact resistance ($R_{C,e}$), and channel resistance ($R_{ch,e}$) for **P6** OFET devices under p- and n-type operation at $V_G = -100$ V and 100 V, respectively, measured under vacuum conditions.

Operation mode	$R_{T,e}$[a] / Ω cm	$R_{C,e}$[b] / Ω cm	$R_{ch,e}$[c] / Ω cm
p-type	4.65×10^7	3.24×10^7	1.41×10^7
n-type	8.47×10^6	5.18×10^6	3.29×10^6

[a] width-normalized total resistance at channel length (L = 100 μm).

[b] width-normalized contact resistance obtained from the y-intercept of the transfer line method (TLM) fitting.

[c] width-normalized channel resistance at L = 100 μm calculated from the TLM fitting.

Table S7 Out-of-plane GIWAXS analysis of higher-order (200), (300), and (400) diffraction peaks for polymers **P1**–**P6**, including peak positions (q_z) and full width at half maximum (FWHM) under the optimized annealing conditions.

Polymer	Annealing	Out-of-plane (200)		Out-of-plane (300)		Out-of-plane (400)	
		q_z / nm^{-1}	FWHM / nm^{-1}	q_z / nm^{-1}	FWHM / nm^{-1}	q_z / nm^{-1}	FWHM / nm^{-1}
P1	300 °C	8.77	0.782	-	-	-	-
P2	300 °C	9.39	1.10	-	-	-	-
P3	300 °C	11.4	0.709				
P4	as cast	4.69	0.620	7.52	0.690	-	-
P5	200 °C	4.70	0.572	7.46	0.680	10.2	0.977
P6	200 °C	5.36	0.653	8.44	0.730	11.6	0.988

5. Spectra

^{1}H NMR (400 MHz, $CDCl_3$) for **Qx-5**

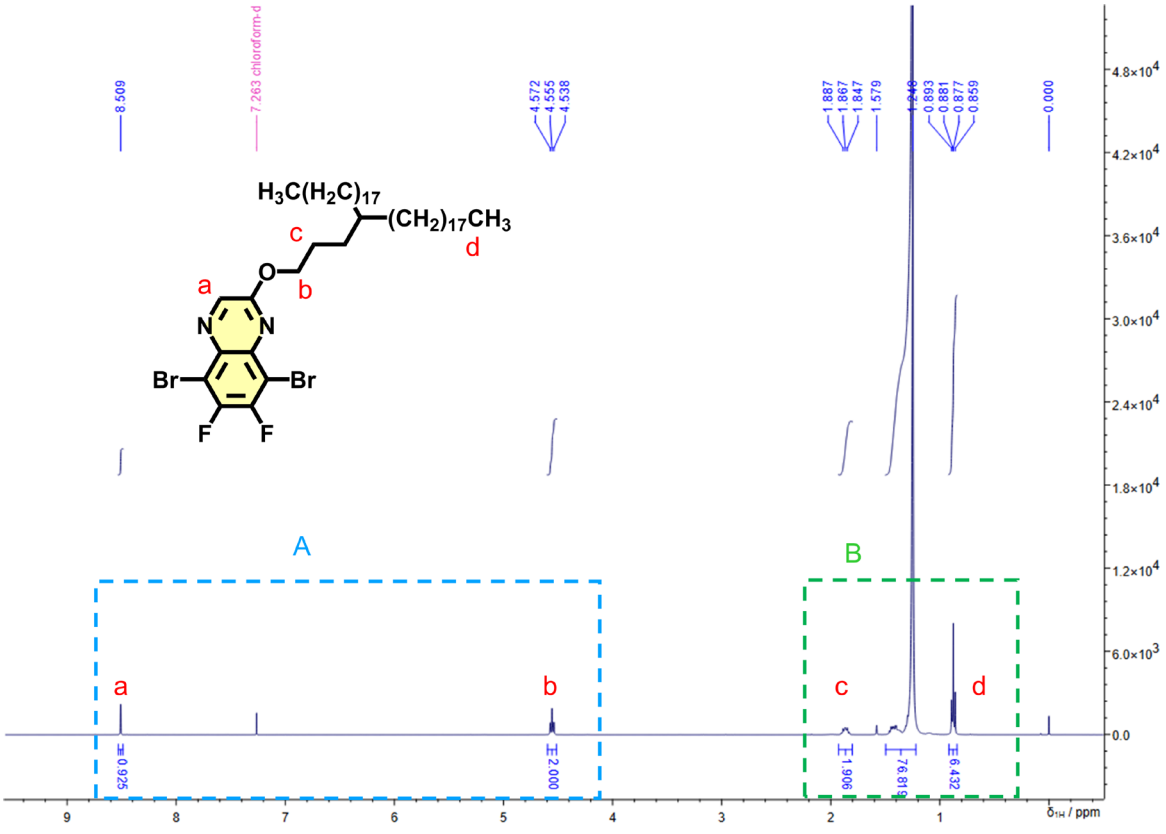

Expanded ^{1}H NMR spectra in the low-field region (**A**)

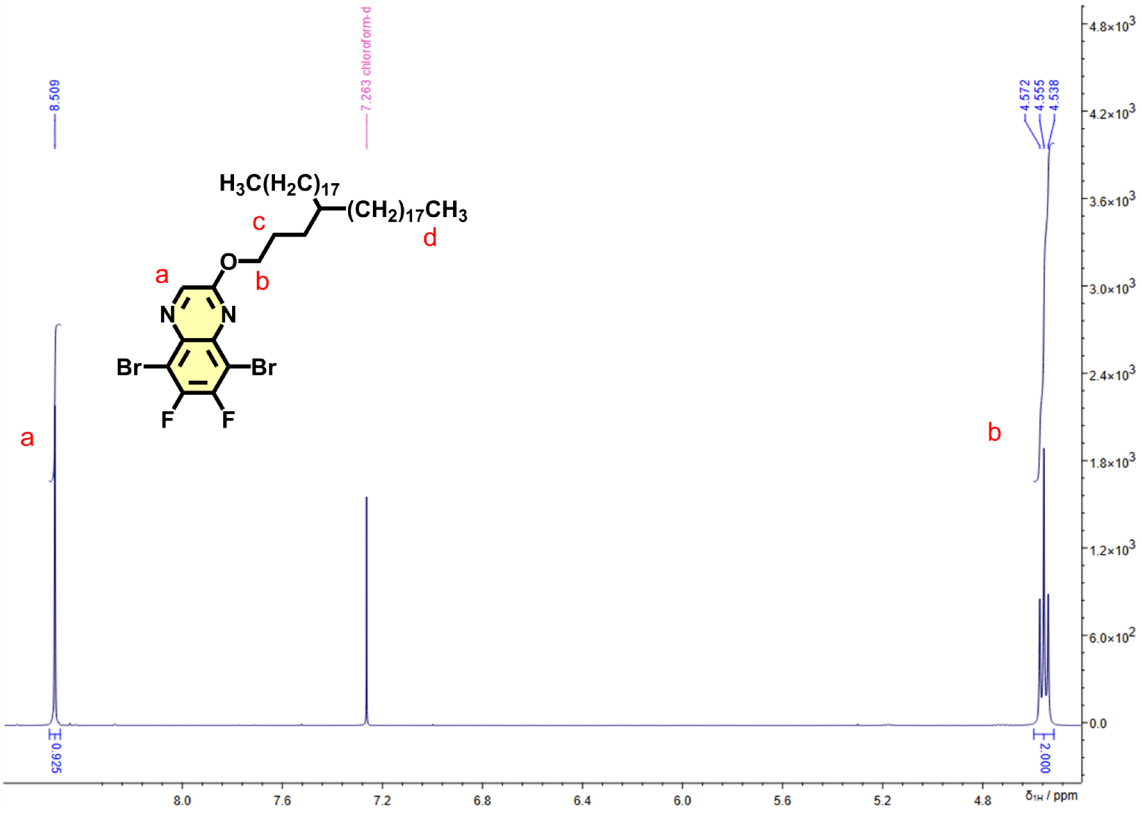

Expanded ^{1}H NMR spectra in the high-field region (**B**)

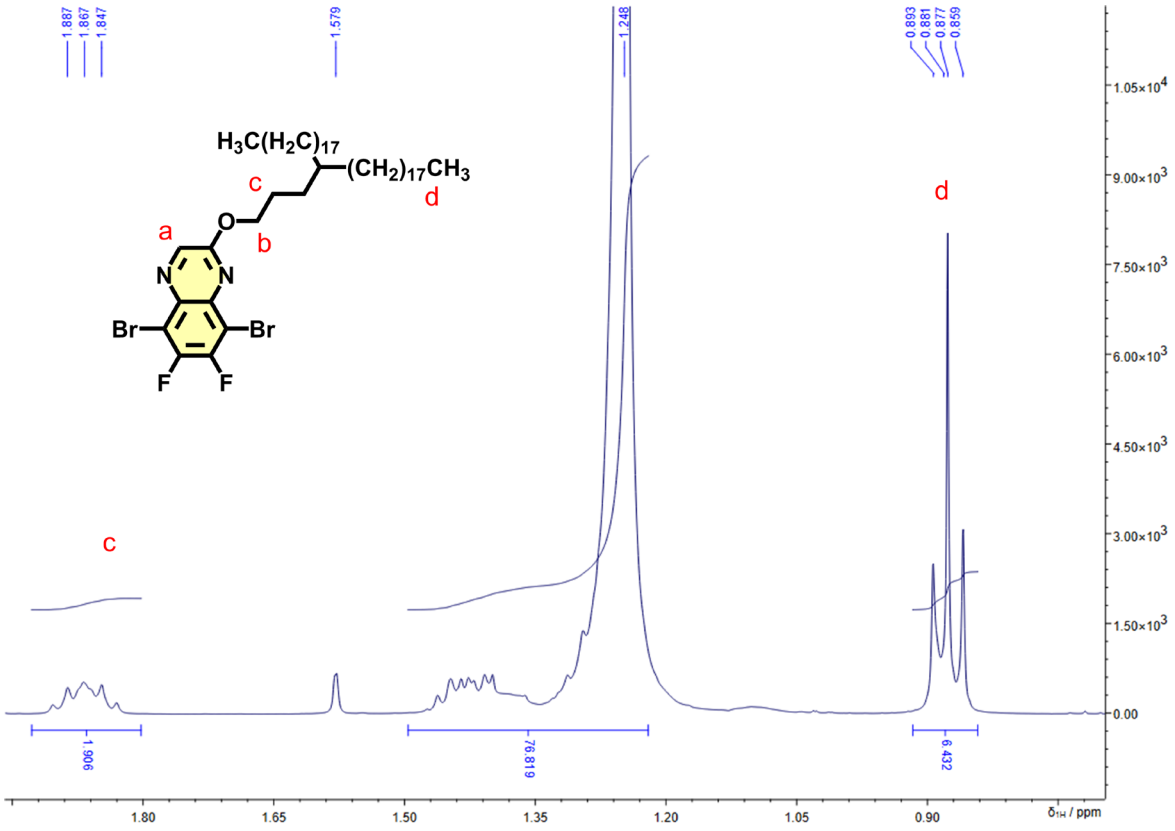

^{1}H-^{1}H COSY for **Qx-5**

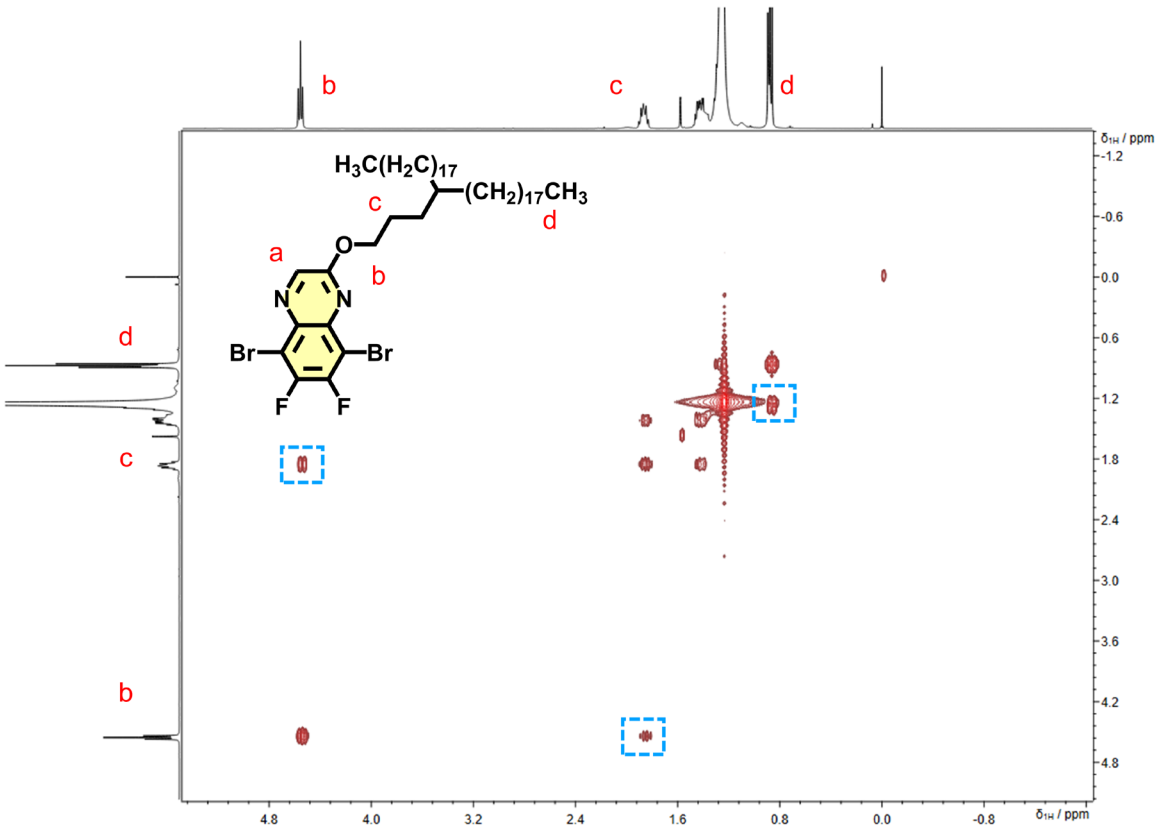

1 ^{13}C NMR (100 MHz, $CDCl_3$) for **Qx-5**

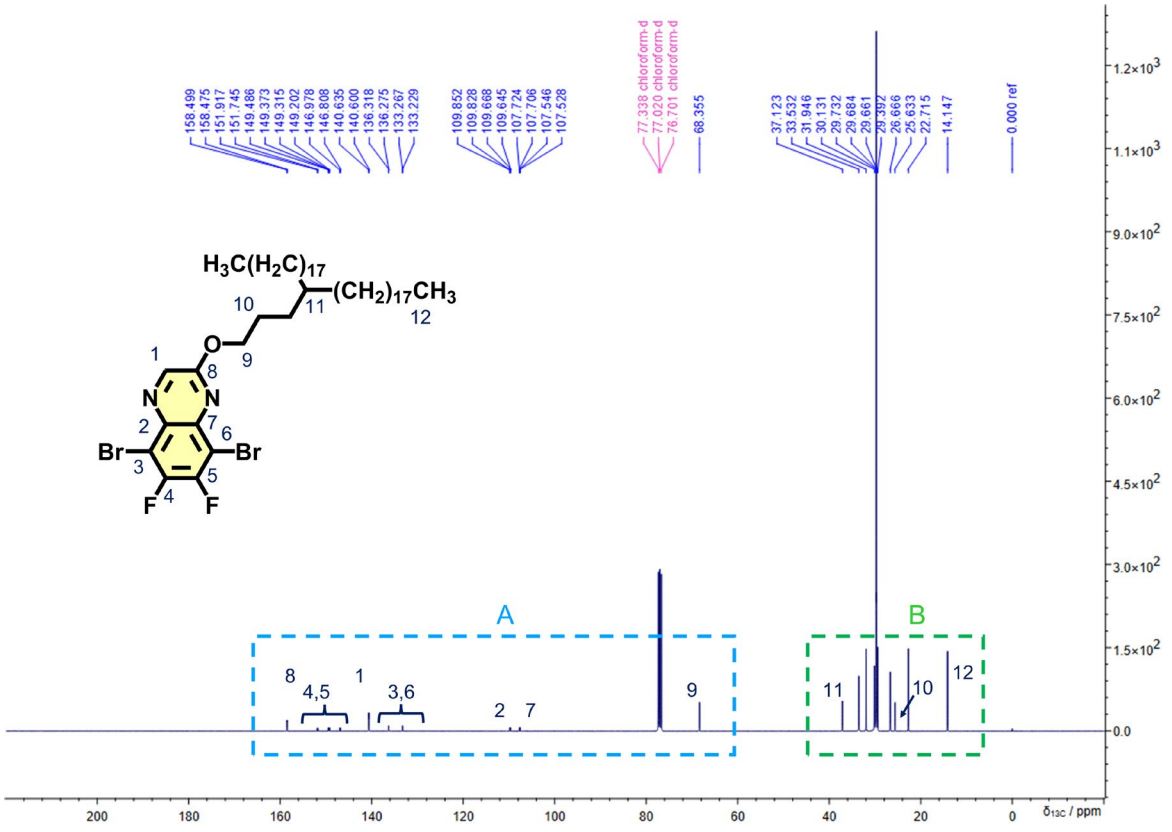

2

3 Expanded ^{13}C NMR spectra in the low-field region (**A**)

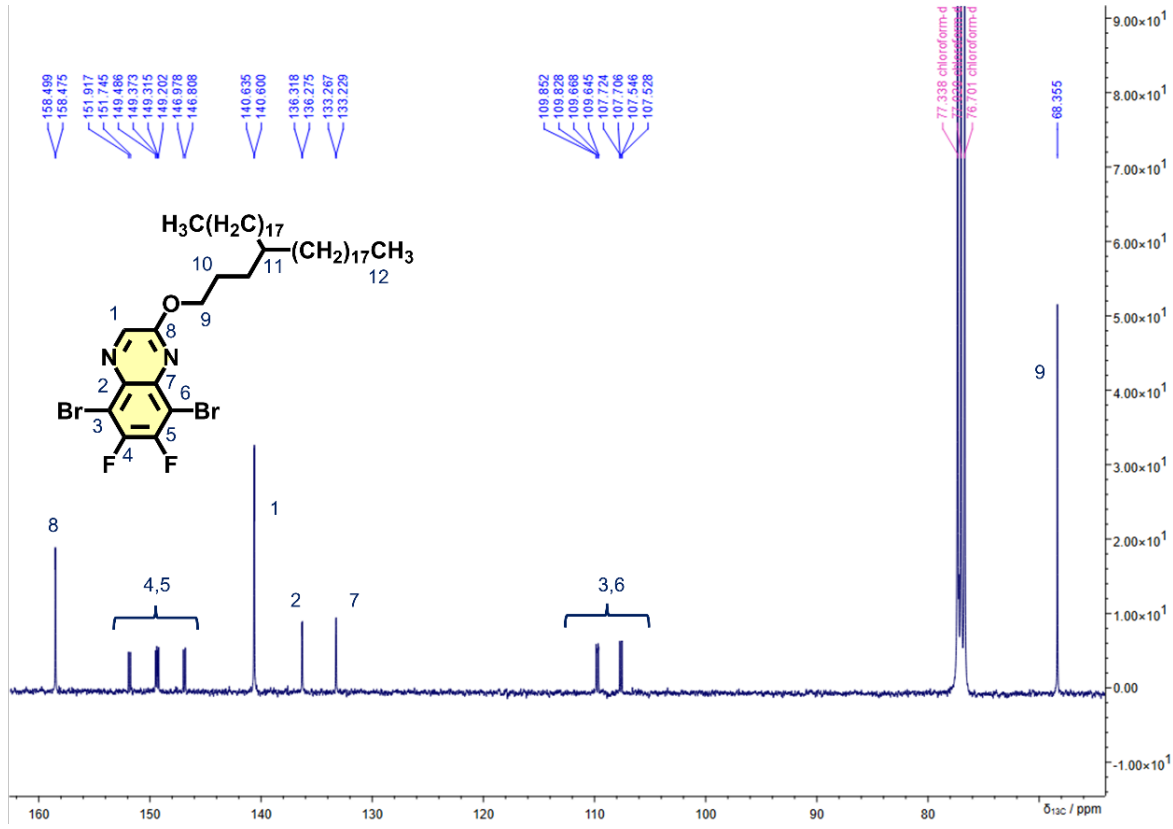

4

Expanded ^{13}C NMR spectra in the high-field region (**B**)

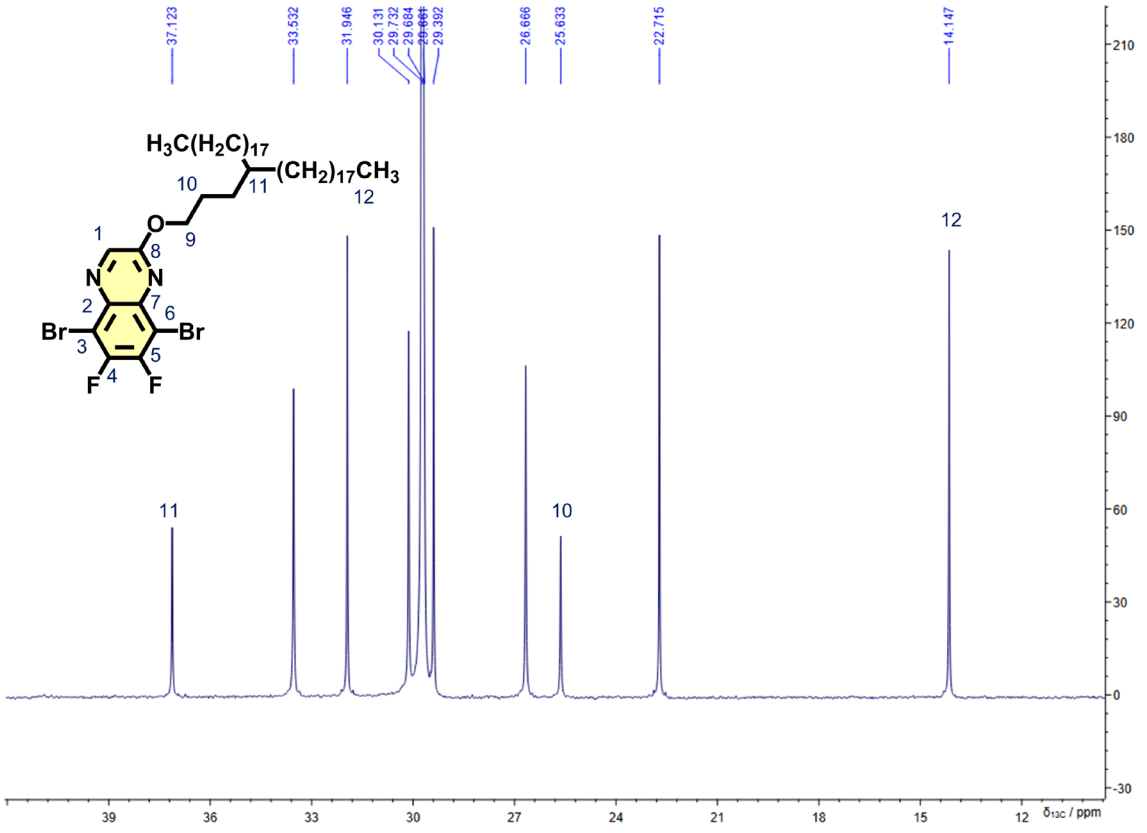

DEPT-135 for **Qx-5**

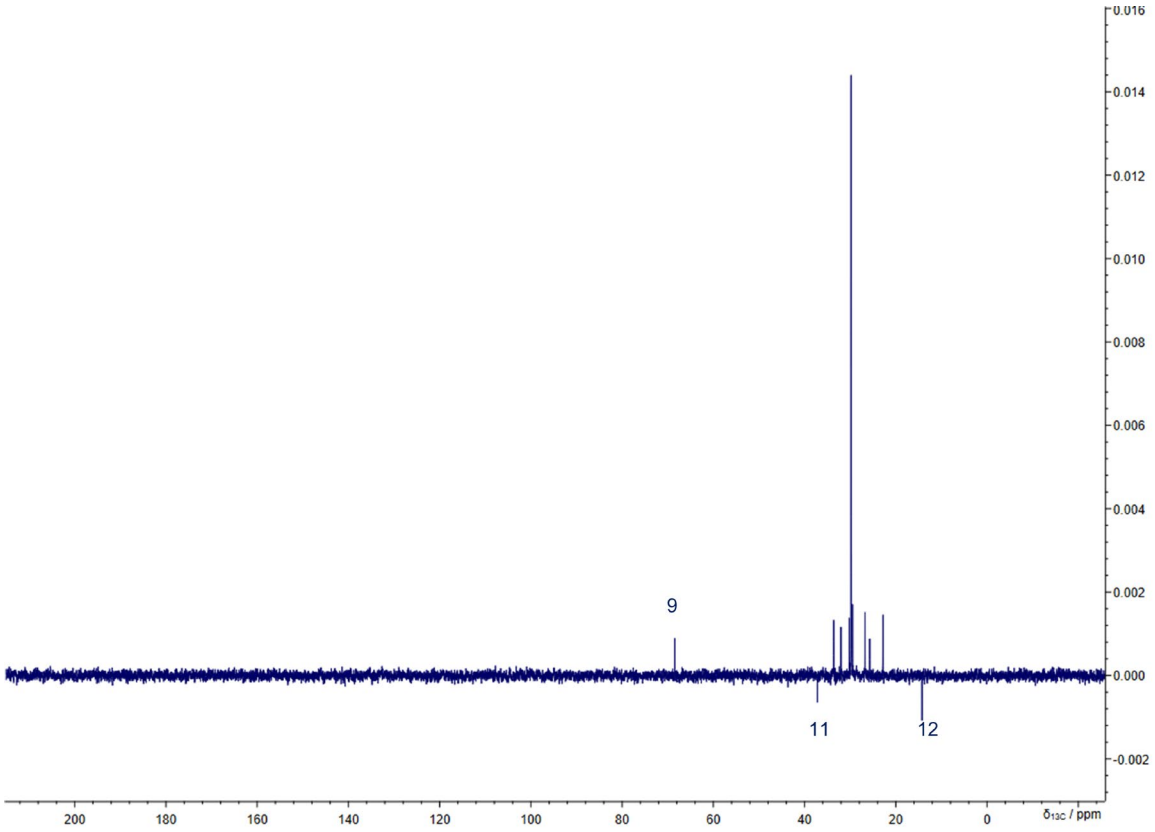

1 gHSQC for **Qx-5**

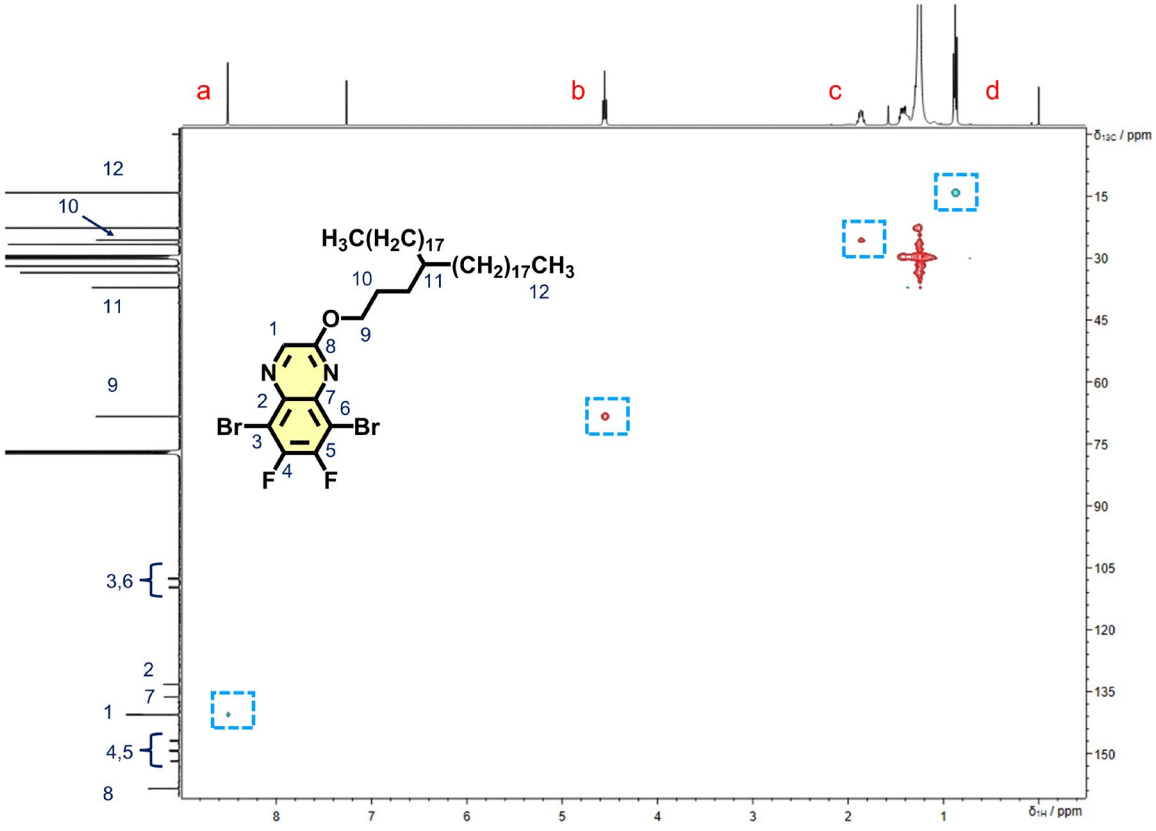

2

3 gHMBC for **Qx-5**

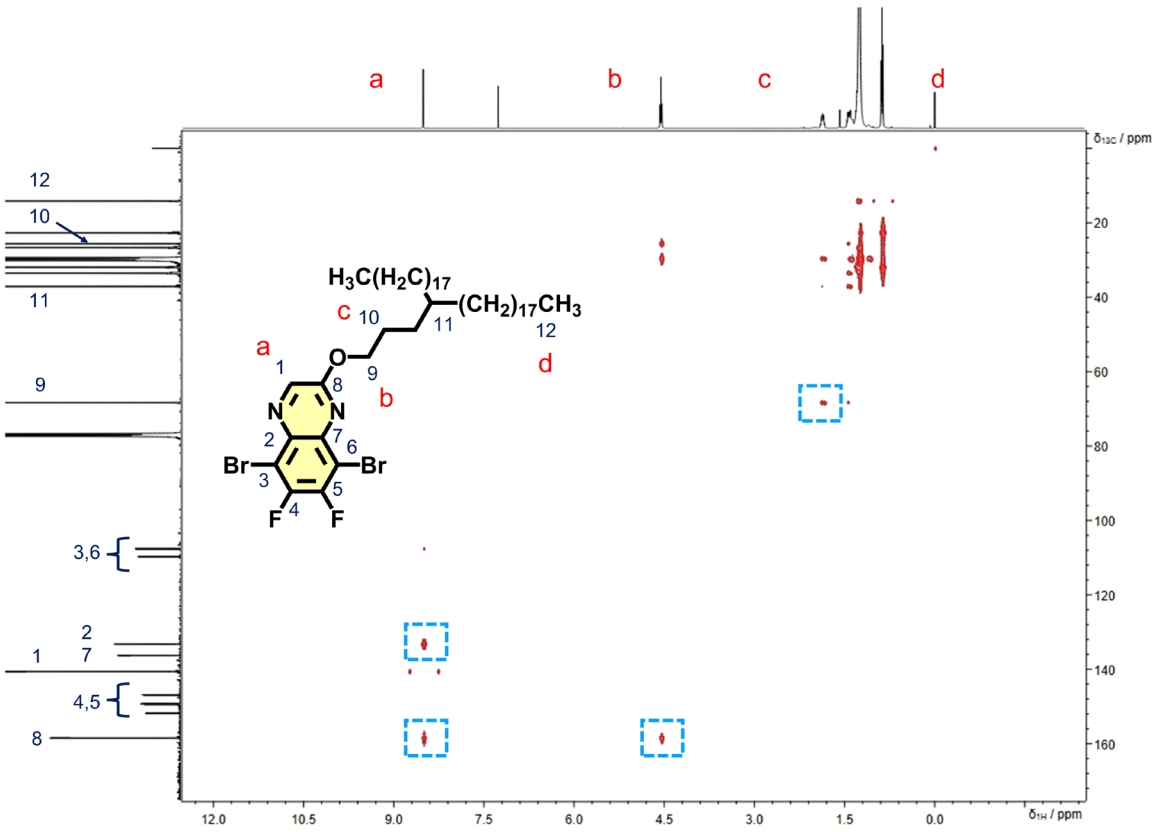

4

^{19}F NMR (376 MHz, $CDCl_3$) for **Qx-5**

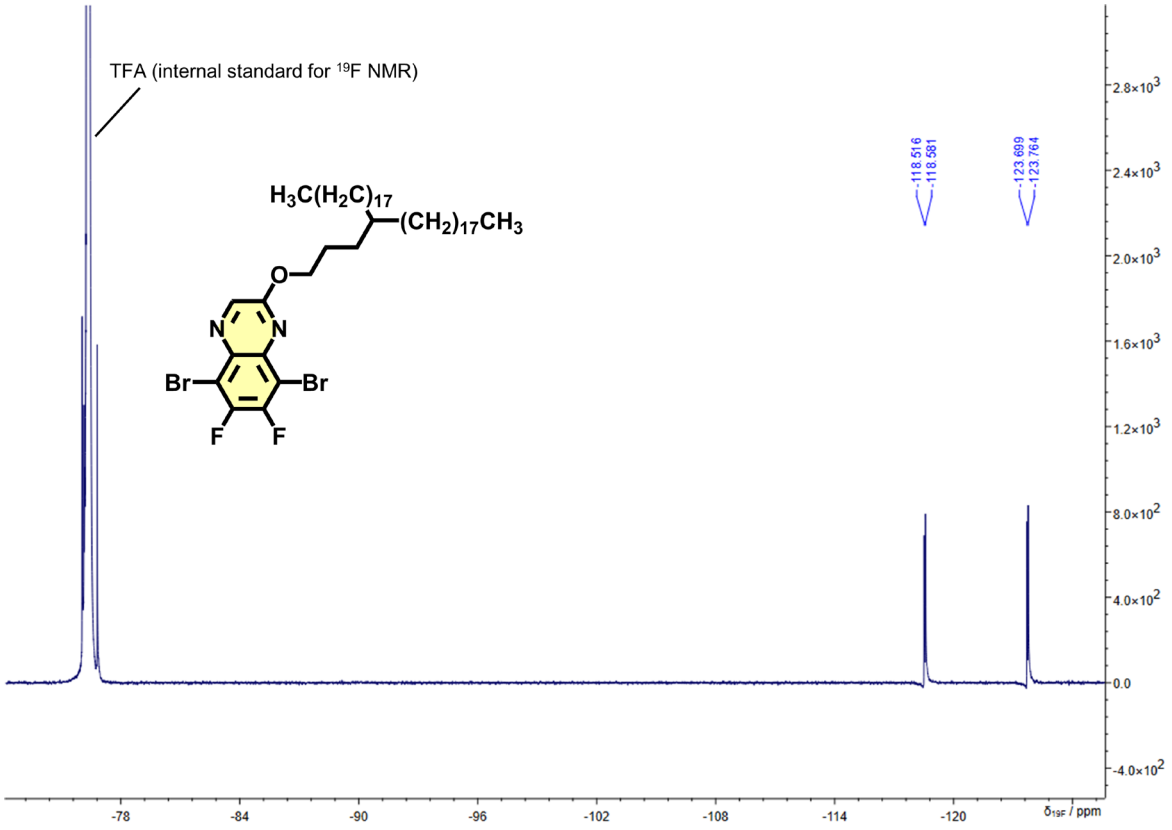

^{1}H NMR (400 MHz, $CDCl_3$) for **P1**

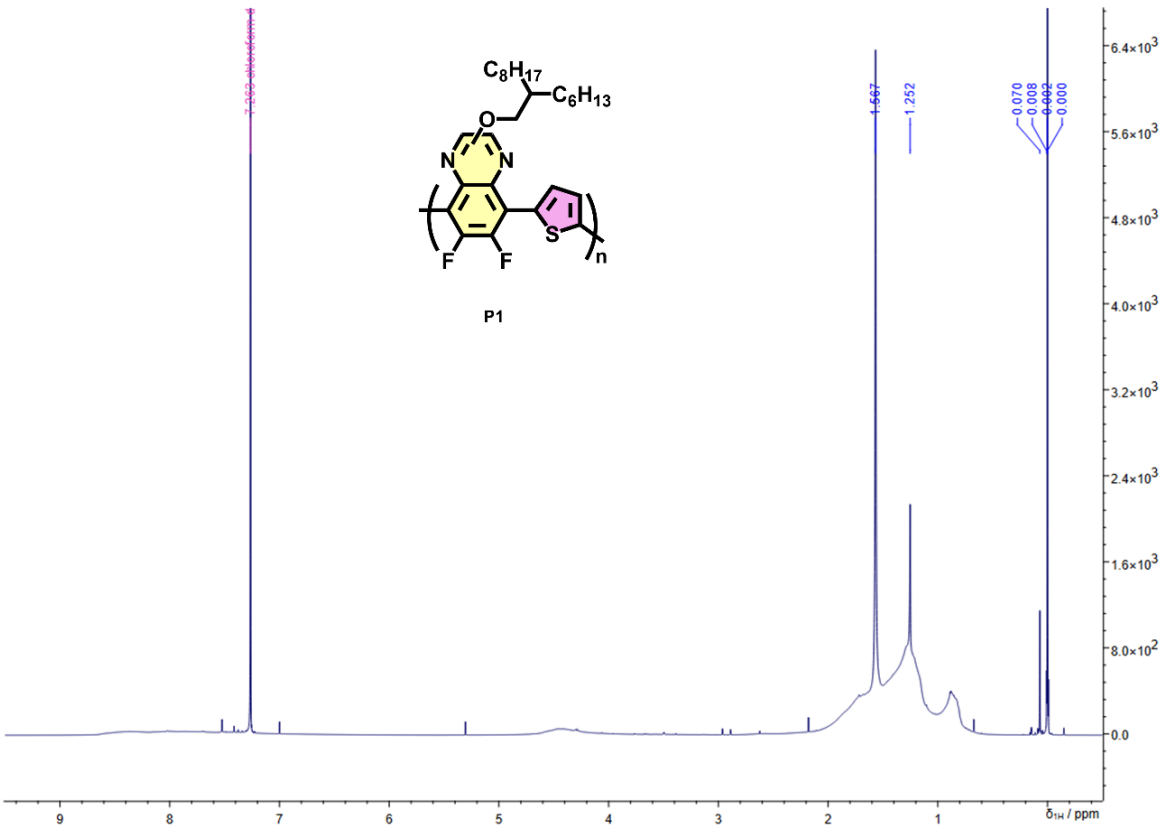

1 ^{1}H NMR (400 MHz, $CDCl_3$) for **P2**

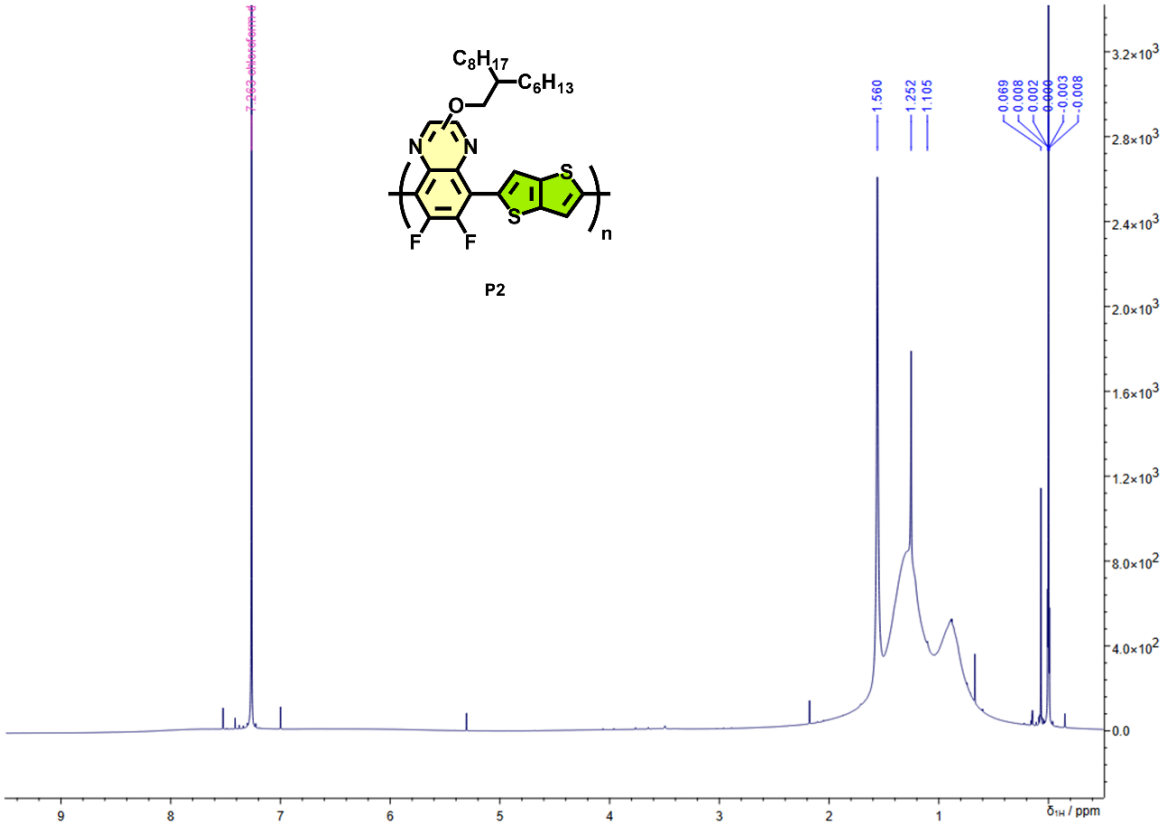

2

3 ^{1}H NMR (400 MHz, $CDCl_3$) for **P3**

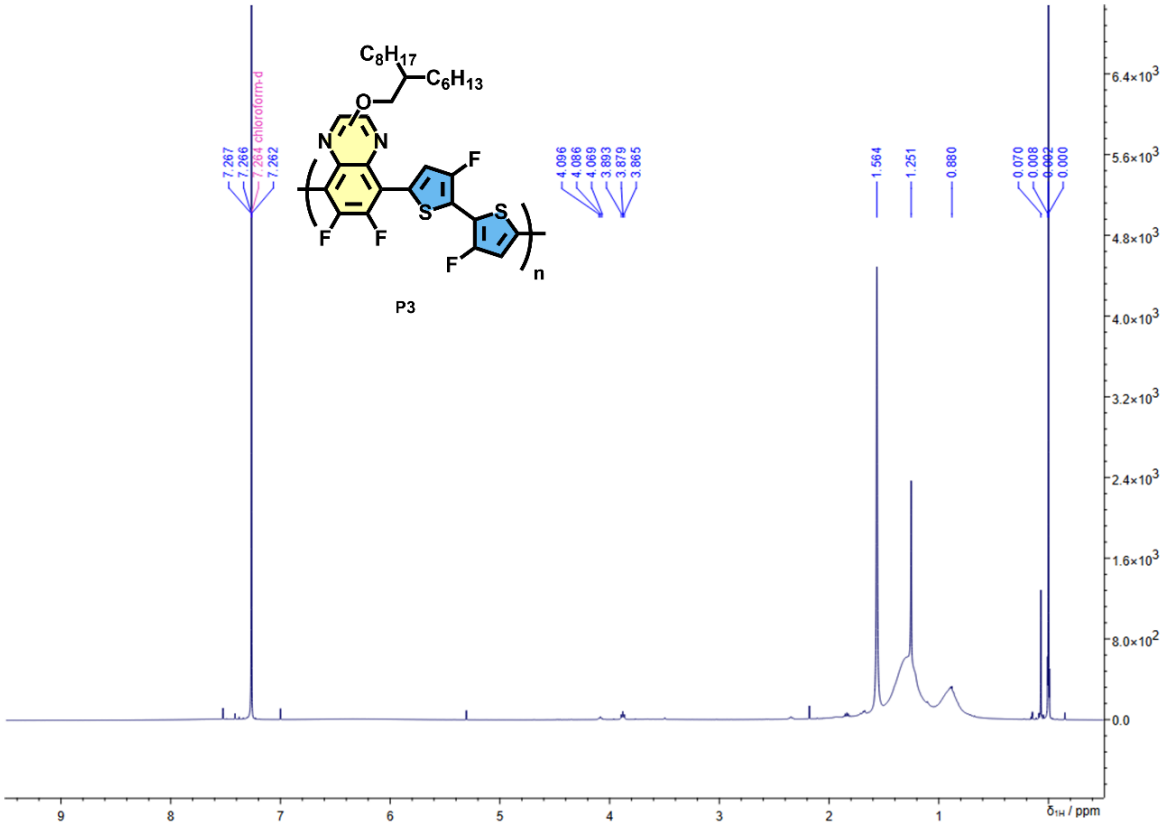

4

1 ^{1}H NMR (400 MHz, $CDCl_3$) for **P4**

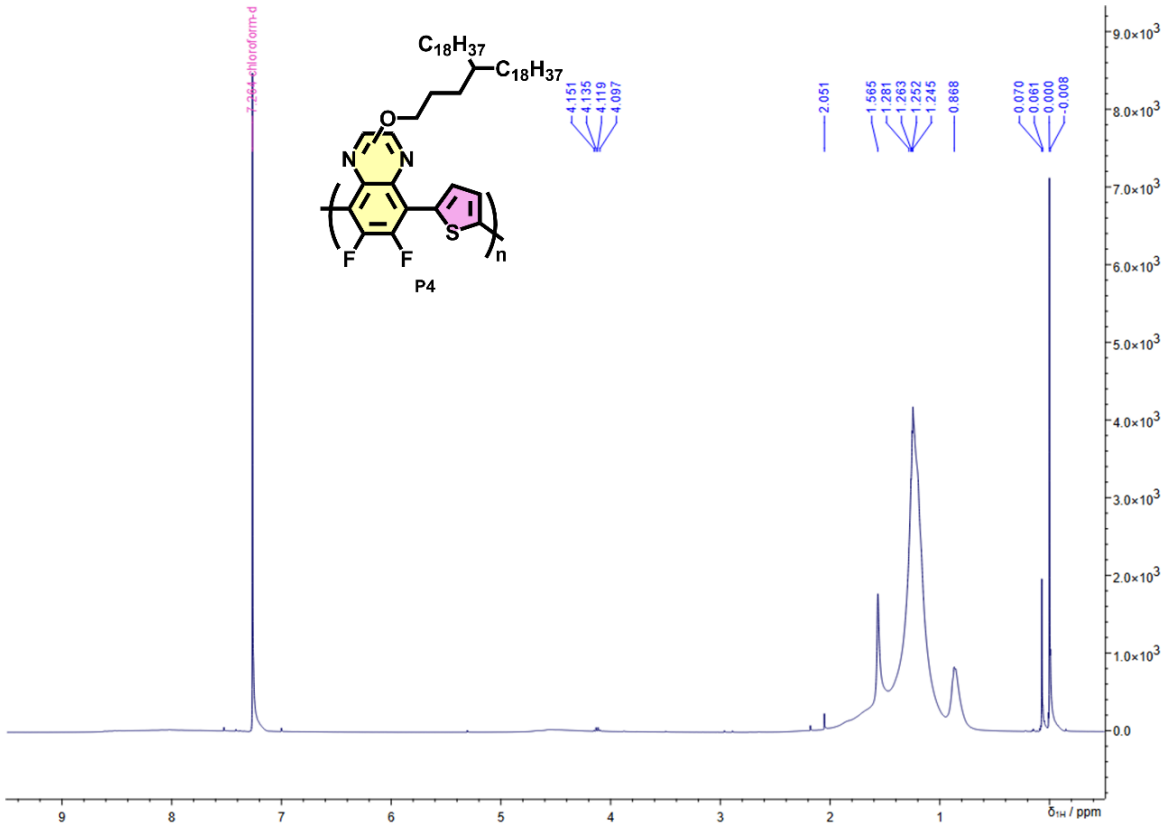

2

3 ^{1}H NMR (400 MHz, $CDCl_3$) for **P5**

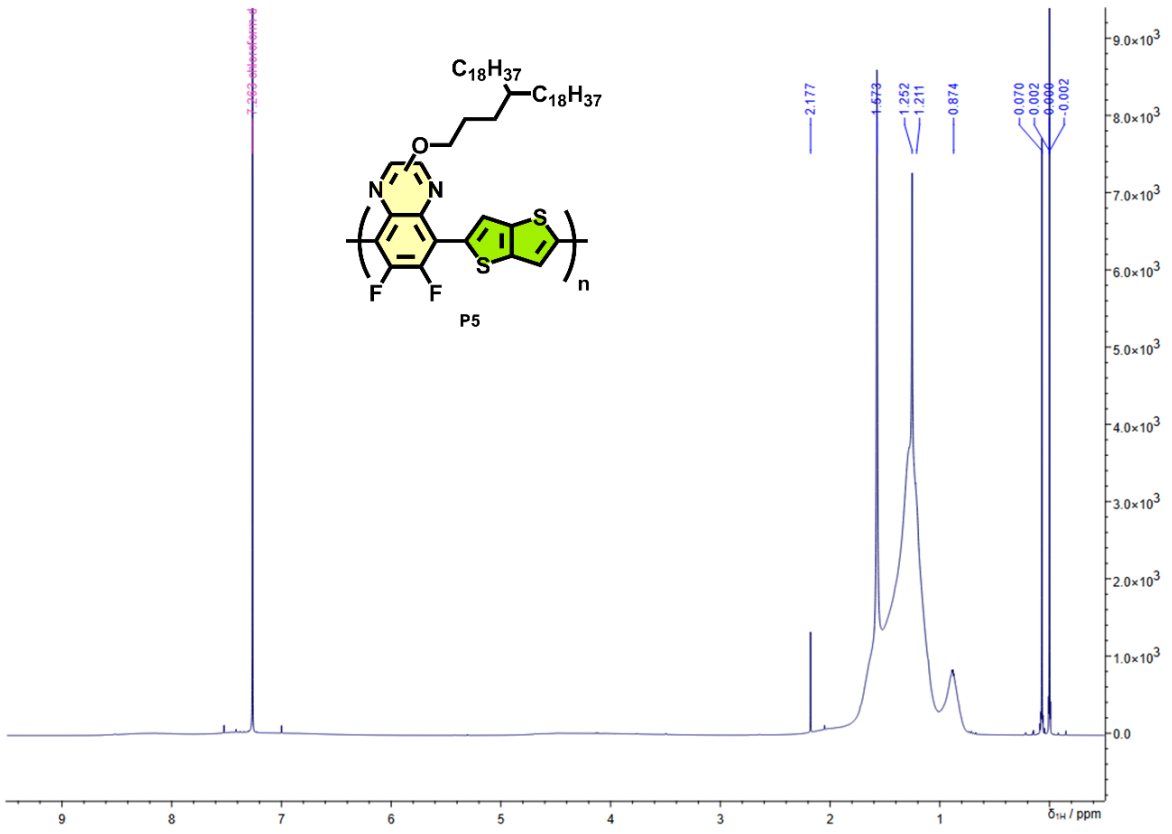

4

^{1}H NMR (400 MHz, $CDCl_3$) for **P6**

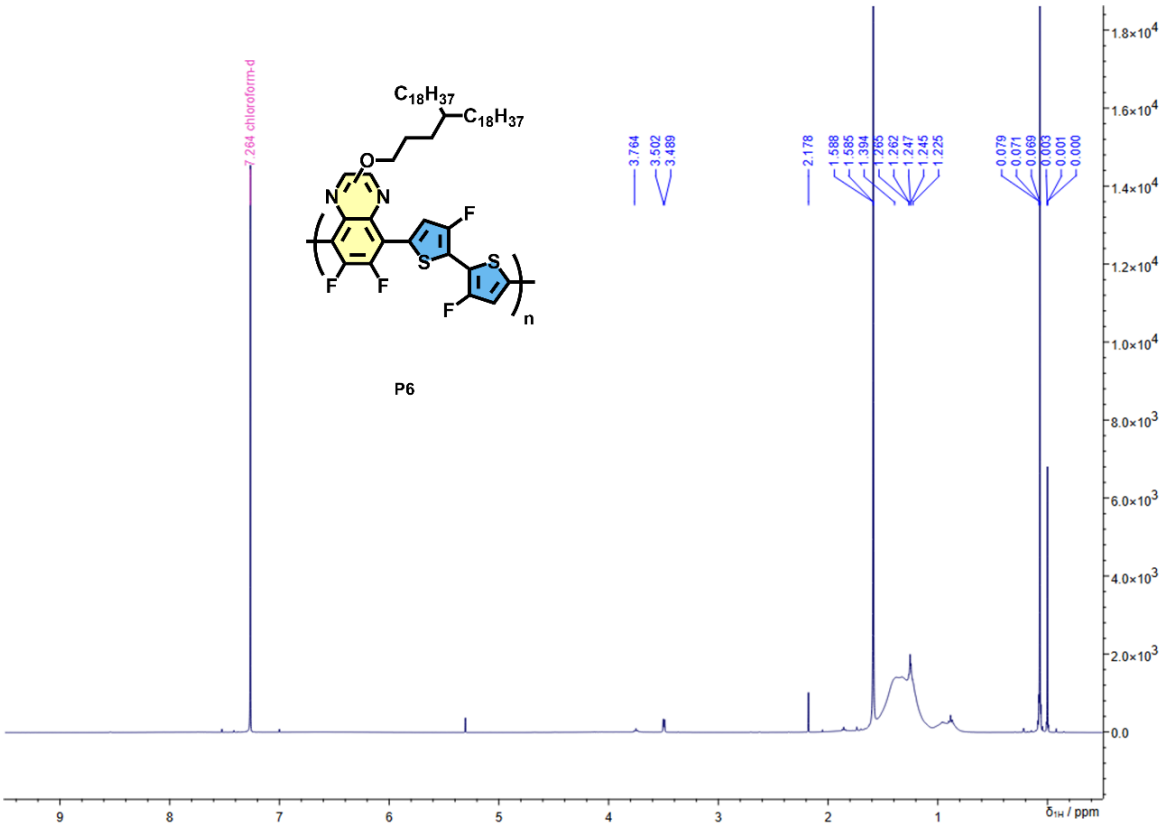

MALDI-TOF-MS for **Qx-5**

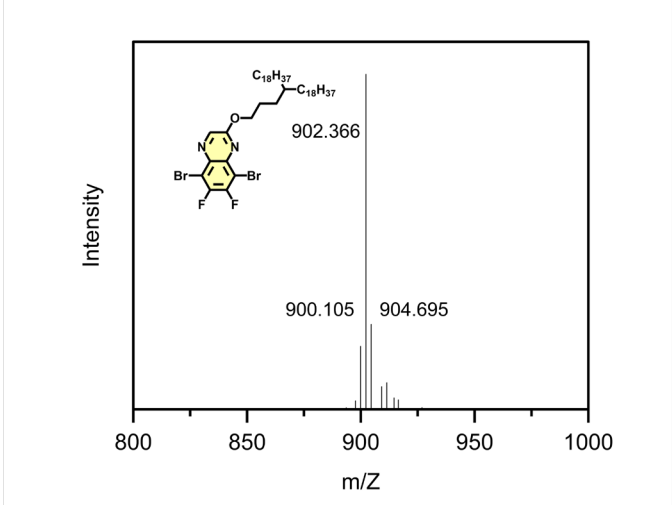

MALDI-TOF-MS for **P1**

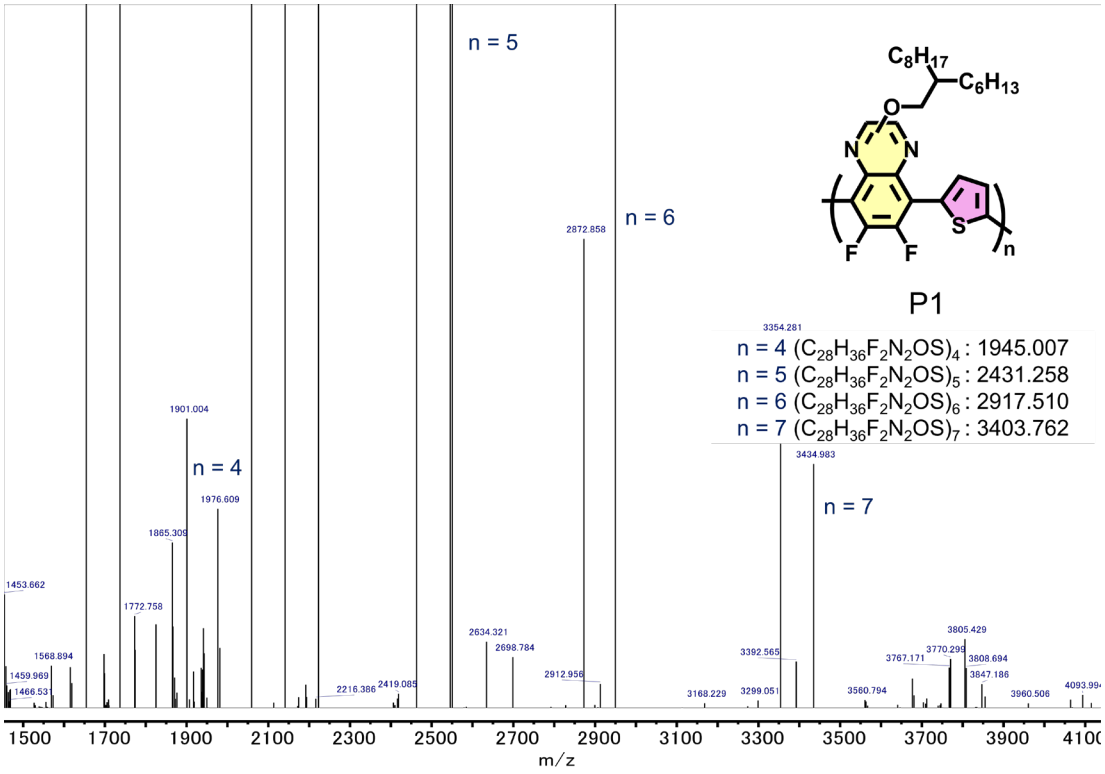

The spacing of the peaks is consistent with a repeating unit mass of 487 Da.

MALDI-TOF-MS for **P2**

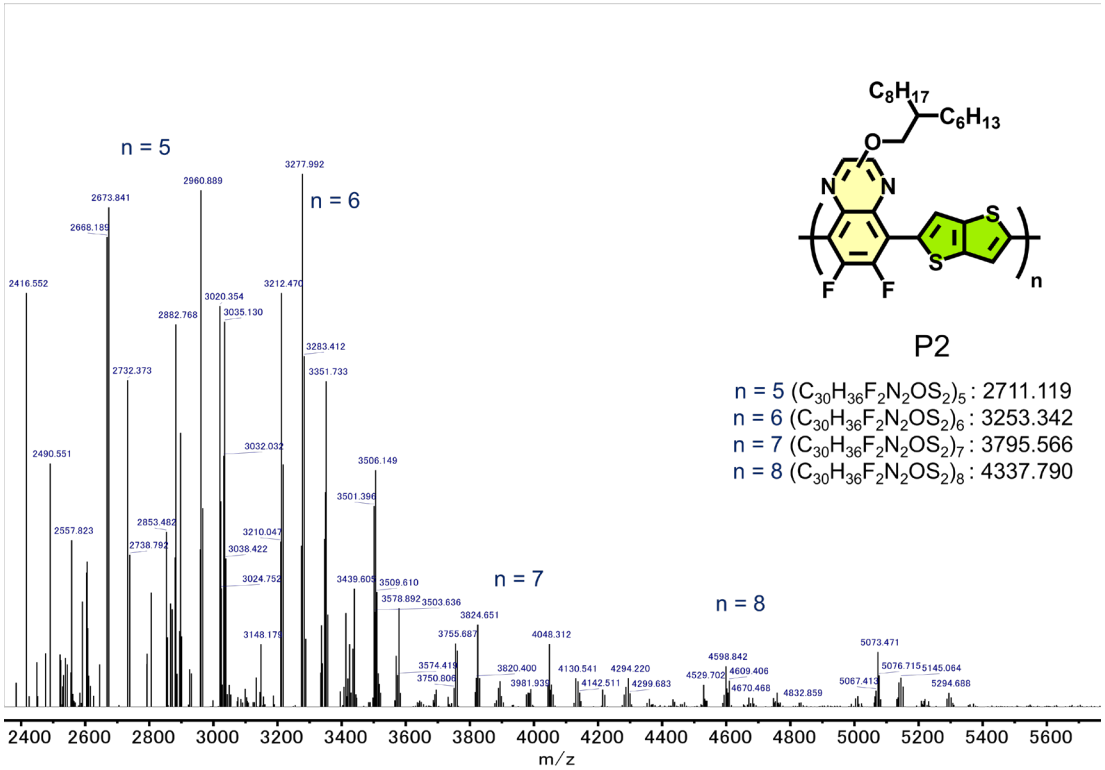

The spacing of the peaks is consistent with a repeating unit mass of approximately 544 Da.

MALDI-TOF-MS for **P3**

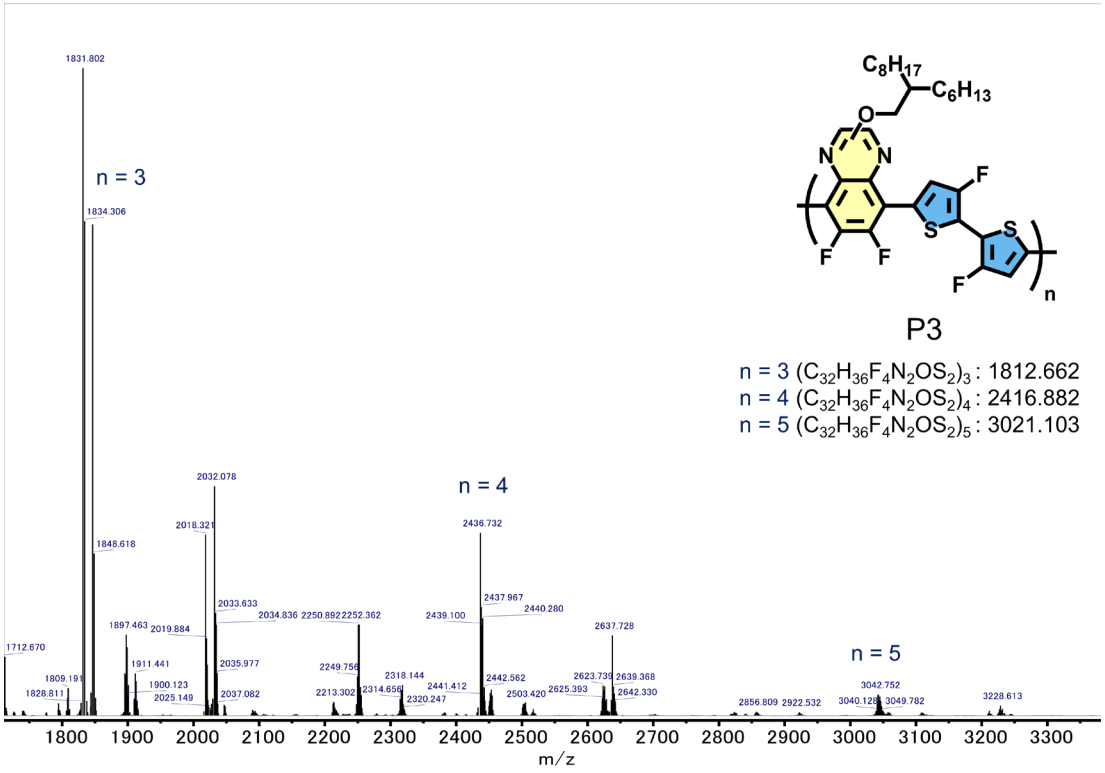

The spacing of the peaks is consistent with a repeating unit mass of approximately 605 Da.

MALDI-TOF-MS for **P4**

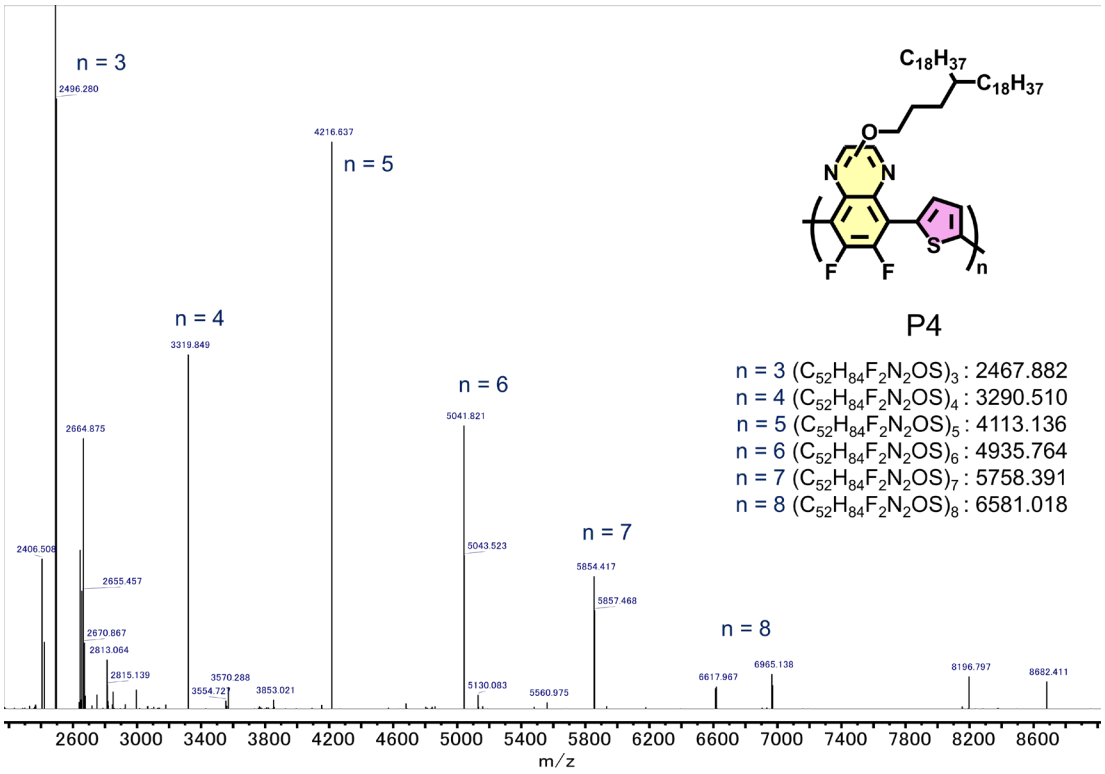

The spacing of the peaks is consistent with a repeating unit mass of approximately 824 Da.

MALDI-TOF-MS for **P5**

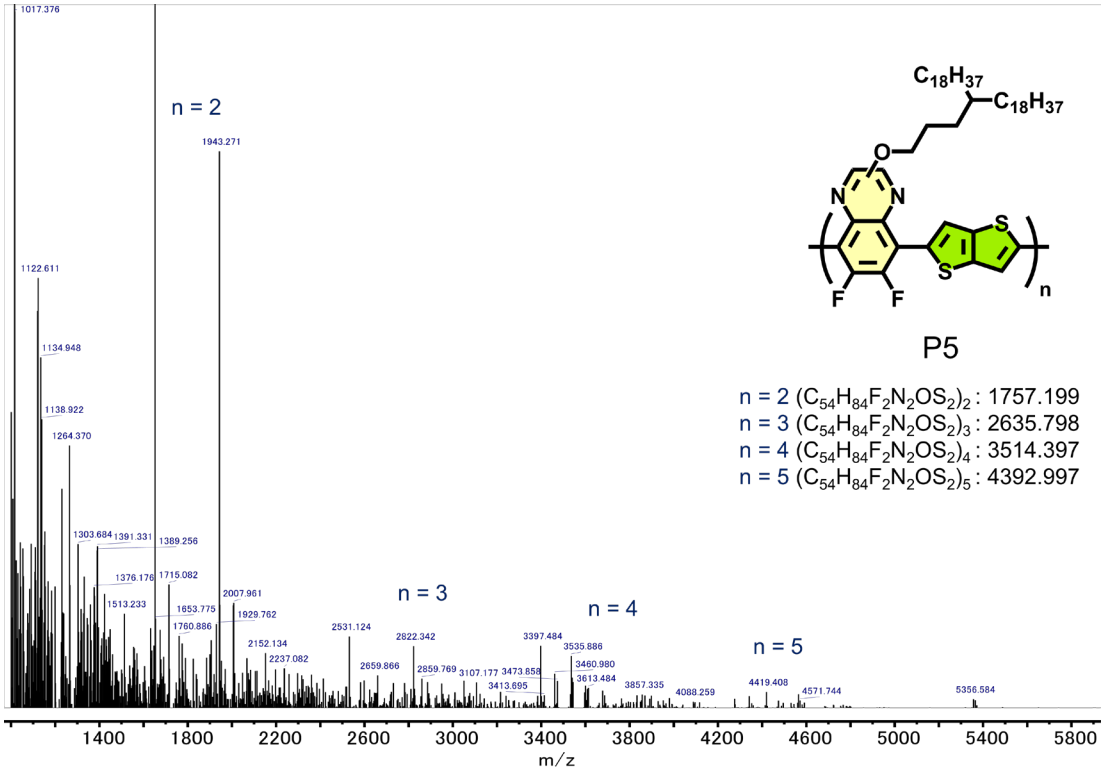

The spacing of the peaks is consistent with a repeating unit mass of approximately 880 Da.

MALDI-TOF-MS for **P6**

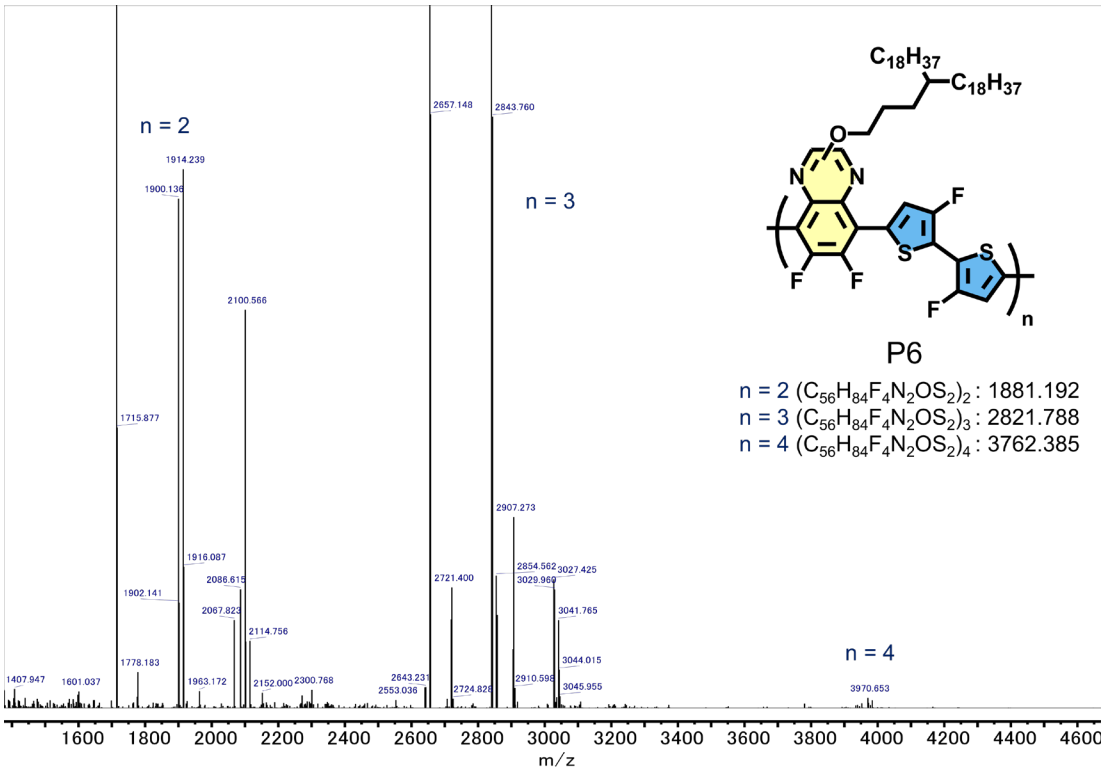

The spacing of the peaks is consistent with a repeating unit mass of approximately 942 Da.

FT-IR Spectra for **Qx-5**

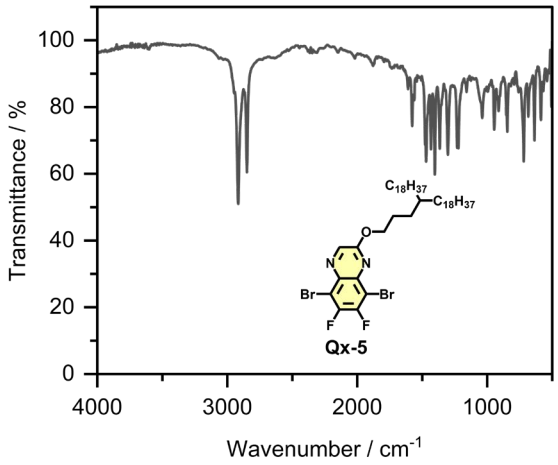

FT-IR Spectra for **P1–P6** (ATR)

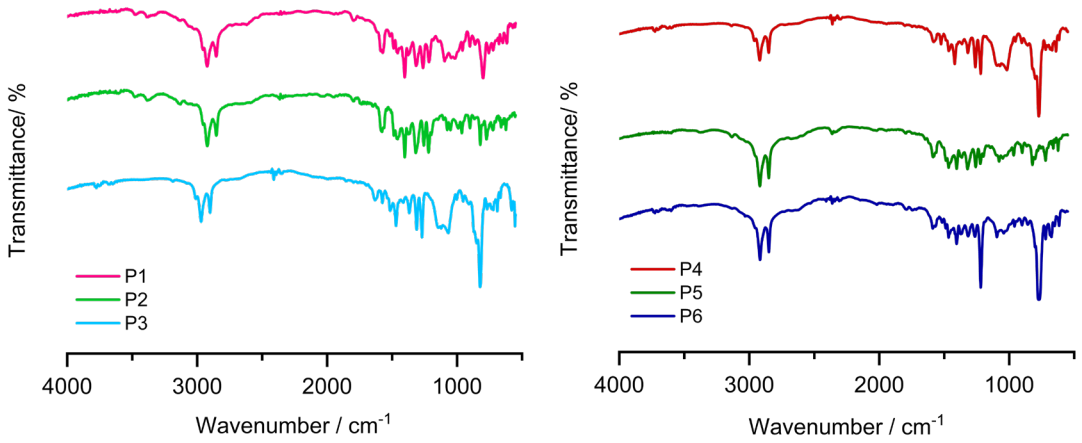

6. Computed Data

Computed data for **P1** and **P4**:

· Method: ωB97XD/6-31G(d,p)

· Total electronic energy: −3845.04432703 a.u.

· Imaginary frequencies: 0

· Cartesian coordinates: (see below)

Center Number	Atomic Number	Atomic Type	X	Y	Z
1	6	0	−7.83813	−0.98719	0.281713
2	6	0	−8.86467	−0.00033	0.501934
3	6	0	−10.1377	−0.3935	0.996341

4	6	0	−10.4215	−1.74961	1.285159
5	6	0	−9.44166	−2.66831	1.078332
6	6	0	−8.17316	−2.28978	0.580656
7	7	0	−8.6095	1.30272	0.244301
8	6	0	−9.56195	2.170147	0.453054
9	6	0	−10.8437	1.777031	0.942622
10	7	0	−11.1152	0.526005	1.206631
11	9	0	−9.63735	−3.96363	1.325851
12	9	0	−7.29607	−3.28132	0.412223
13	6	0	−4.05787	−0.46726	−0.71488
14	6	0	−4.80328	0.48542	−1.36207
15	6	0	−6.18713	0.396306	−1.09084
16	6	0	−6.50956	−0.62743	−0.23338
17	16	0	−5.0798	−1.50195	0.226734
18	6	0	0.28736	−1.02229	−0.84328
19	6	0	−0.29989	0.283971	−0.78422
20	6	0	−1.70513	0.476121	−0.74068
21	6	0	−2.00485	−1.87926	−0.78465
22	6	0	−0.61141	−2.06908	−0.82095
23	7	0	0.532312	1.36163	−0.76457
24	6	0	0.017867	2.552478	−0.69452
25	6	0	−1.39673	2.733205	−0.64315
26	7	0	−2.22529	1.732146	−0.67097
27	9	0	−2.74301	−2.99037	−0.78187
28	9	0	−0.21151	−3.34417	−0.83808
29	6	0	−2.60006	−0.63896	−0.74809
30	6	0	8.45269	−0.47153	0.311899
31	6	0	7.5176	0.615435	0.195541
32	6	0	6.14829	0.373472	−0.11264
33	6	0	5.628493	−0.94802	−0.33043
34	6	0	6.552533	−1.95651	−0.18522
35	6	0	7.910948	−1.71963	0.111715
36	7	0	7.95106	1.879104	0.395692
37	6	0	7.099121	2.862881	0.298676
38	6	0	5.729894	2.62829	−0.00702
39	7	0	5.291377	1.413696	−0.20392
40	9	0	6.224135	−3.24426	−0.32293
41	9	0	8.666291	−2.81721	0.204075

42	6	0	12.22189	−0.51718	1.424107
43	6	0	11.98714	0.696906	0.849981
44	6	0	10.64881	0.838822	0.398059
45	6	0	9.87484	−0.27455	0.62235
46	16	0	10.82653	−1.51444	1.403302
47	16	0	2.920443	−0.13389	−0.32361
48	6	0	1.734569	−1.26567	−0.90202
49	6	0	2.346938	−2.39957	−1.38836
50	6	0	3.748664	−2.38006	−1.25366
51	6	0	4.22633	−1.2315	−0.66064
52	8	0	−9.235	3.443813	0.171963
53	6	0	−10.2043	4.455894	0.375781
54	8	0	−1.83594	3.992337	−0.55959
55	6	0	−3.25011	4.165833	−0.50867
56	8	0	7.619951	4.083512	0.508099
57	6	0	6.760658	5.206904	0.43683
58	1	0	−11.3964	−2.03153	1.661799
59	1	0	−11.6364	2.498278	1.114796
60	1	0	−4.36153	1.23223	−2.0062
61	1	0	−6.92474	1.074197	−1.49328
62	1	0	0.680991	3.412883	−0.67597
63	1	0	5.005436	3.432248	−0.08913
64	1	0	13.14495	−0.8898	1.845225
65	1	0	12.73931	1.469495	0.751934
66	1	0	10.25646	1.735881	−0.05568
67	1	0	1.809414	−3.22423	−1.83189
68	1	0	4.383129	−3.18795	−1.58541
69	1	0	−9.72135	5.3894	0.089879
70	1	0	−11.088	4.302518	−0.25412
71	1	0	−10.5093	4.517728	1.426658
72	1	0	−3.40747	5.236088	−0.38314
73	1	0	−3.71585	3.81946	−1.43534
74	1	0	−3.68334	3.609328	0.325852
75	1	0	7.387991	6.072644	0.644496
76	1	0	6.318869	5.314835	−0.56047
77	1	0	5.963686	5.153235	1.187305

Computed data for **P2** and **P5**:

· Method: ωB97XD/6-31G(d,p)

· Total electronic energy: − 5268.11567605 a.u.

· Imaginary frequencies: 0

· Cartesian coordinates: (see below)

Center Number	Atomic Number	Atomic Type	X	Y	Z
1	7	0	0.894649	1.796504	1.004002
2	6	0	1.615622	2.783812	1.442832
3	6	0	3.040052	2.698998	1.437502
4	7	0	3.670055	1.649229	1.000002
5	9	0	3.305411	−2.74856	−0.76646
6	9	0	0.762188	−2.62986	−0.75418
7	6	0	1.512982	0.675736	0.542159
8	6	0	2.930013	0.602554	0.542488
9	6	0	3.605785	−0.5719	0.08347
10	6	0	2.78809	−1.59859	−0.33115
11	6	0	1.383647	−1.52607	−0.32582
12	6	0	0.689383	−0.40318	0.078706
13	6	0	11.13103	−0.98887	0.209874
14	6	0	12.02618	−0.05606	−0.42298
15	6	0	13.43377	−0.21	−0.32371
16	6	0	13.99564	−1.27833	0.412795
17	6	0	13.14468	−2.14366	1.024709
18	6	0	11.74075	−1.99729	0.930962
19	7	0	11.50539	0.981153	−1.11193
20	6	0	12.32208	1.824477	−1.68263
21	6	0	13.73799	1.662486	−1.5959
22	7	0	14.27058	0.671135	−0.93082
23	9	0	13.5977	−3.16902	1.747063
24	9	0	11.03363	−2.91282	1.598626
25	6	0	9.667269	−0.88368	0.116401
26	6	0	8.766308	−1.88132	0.413259
27	6	0	7.426631	−1.44181	0.293787
28	6	0	7.305469	−0.11905	−0.08919
29	16	0	8.850854	0.609507	−0.35208
30	16	0	5.877007	−2.18373	0.489328

31	6	0	5.06964	−0.67932	0.064472
32	6	0	5.962893	0.319231	−0.22166
33	6	0	−0.77815	−0.34738	0.043113
34	6	0	−1.59809	−1.20253	−0.65906
35	6	0	−2.96814	−0.92557	−0.4417
36	6	0	−3.19497	0.12311	0.430056
37	16	0	−1.71201	0.829777	0.969369
38	16	0	−4.45263	−1.61298	−0.99788
39	6	0	−5.38023	−0.44636	−0.05888
40	6	0	−4.5676	0.406136	0.64388
41	6	0	−9.77959	−0.48765	−0.15096
42	6	0	−9.04411	0.73975	−0.0135
43	6	0	−7.62149	0.768193	0.01258
44	6	0	−7.58302	−1.58632	−0.25607
45	6	0	−8.9928	−1.61024	−0.29296
46	7	0	−9.74745	1.886323	0.08087
47	6	0	−9.10784	3.018313	0.190756
48	6	0	−7.68514	3.053883	0.212596
49	7	0	−6.98138	1.955998	0.124548
50	9	0	−6.98922	−2.77545	−0.38789
51	9	0	−9.52116	−2.82449	−0.46446
52	6	0	−11.2468	−0.55606	−0.16058
53	6	0	−12.0006	−1.69739	−0.00319
54	6	0	−13.3868	−1.44175	−0.12795
55	6	0	−13.6911	−0.1181	−0.38552
56	16	0	−12.2667	0.858295	−0.43915
57	16	0	−14.8254	−2.40706	−0.02848
58	6	0	−15.8099	−1.00583	−0.33331
59	6	0	−15.0902	0.137337	−0.49993
60	6	0	−6.84702	−0.43749	−0.1009
61	8	0	3.702619	3.755797	1.913413
62	6	0	5.125568	3.667628	1.90891
63	8	0	11.72757	2.83175	−2.34004
64	6	0	12.53825	3.790297	−2.99641
65	8	0	−9.88725	4.10619	0.27575
66	6	0	−9.26945	5.375671	0.393738

67	1	0	1.119212	3.675077	1.815997
68	1	0	15.07007	−1.38843	0.482602
69	1	0	14.42185	2.355692	−2.07549
70	1	0	9.054369	−2.87874	0.704613
71	1	0	5.655972	1.317602	−0.49529
72	1	0	−1.23192	−1.988	−1.30049
73	1	0	−4.95039	1.200662	1.265932
74	1	0	−7.13371	3.985363	0.294245
75	1	0	−11.5791	−2.6701	0.193103
76	1	0	−16.8847	−1.11374	−0.37471
77	1	0	−15.5344	1.104082	−0.69733
78	1	0	5.475073	4.578593	2.392248
79	1	0	5.464544	2.784082	2.455034
80	1	0	5.505812	3.612561	0.885023
81	1	0	11.84708	4.497009	−3.45332
82	1	0	13.18353	4.32483	−2.29
83	1	0	13.15162	3.331132	−3.77991
84	1	0	−10.0843	6.095975	0.448912
85	1	0	−8.66527	5.446488	1.305345
86	1	0	−8.64692	5.603597	−0.47889

Computed data for **P3** and **P6**:

· Method: ωB97XD/6-31G(d,p)

· Total electronic energy: −6095.51679943 a.u.

· Imaginary frequencies: 0

· Cartesian coordinates: (see below)

Center Number	**Atomic Number**	**Atomic Type**	**X**	**Y**	**Z**
1	6	0	11.57914	0.815993	0.119661
2	6	0	12.96672	0.514668	0.103679
3	6	0	13.44623	−0.83074	0.196873
4	6	0	12.4632	−1.7969	0.258532
5	6	0	11.08953	−1.50086	0.276789
6	7	0	11.16641	2.112242	0.020615
7	6	0	12.06077	3.048478	−0.07978
8	6	0	13.45346	2.737003	−0.0935

9	7	0	13.88552	1.512587	−0.00819
10	9	0	12.76068	−3.09614	0.31585
11	9	0	10.27554	−2.55777	0.351855
12	6	0	17.3457	−1.33994	−0.10478
13	6	0	16.80548	−2.43536	0.489984
14	6	0	15.40468	−2.37336	0.67636
15	6	0	14.87012	−1.19224	0.218762
16	16	0	16.12917	−0.16682	−0.42257
17	9	0	17.51654	−3.49722	0.879627
18	6	0	6.646889	−0.06256	0.010442
19	6	0	7.120942	1.102408	0.556755
20	6	0	8.5185	1.189399	0.697923
21	6	0	9.148921	0.05317	0.255801
22	16	0	7.987989	−1.11384	−0.32375
23	9	0	6.313201	2.100954	0.936198
24	6	0	4.812863	−1.59957	−0.80578
25	6	0	3.417531	−1.69475	−0.93936
26	16	0	3.927568	0.602237	0.116117
27	9	0	5.625434	−2.58771	−1.20301
28	6	0	5.274367	−0.43819	−0.24679
29	6	0	10.59028	−0.21907	0.217783
30	6	0	−0.69414	1.080169	−0.05735
31	6	0	0.711457	0.887596	−0.07108
32	6	0	1.31869	−0.35711	−0.44272
33	6	0	0.421658	−1.35778	−0.76023
34	6	0	−0.97128	−1.17021	−0.74885
35	7	0	−1.21402	2.282128	0.314065
36	6	0	−0.39003	3.228206	0.657543
37	6	0	1.025077	3.046279	0.644718
38	7	0	1.536242	1.907482	0.287126
39	9	0	0.817062	−2.58529	−1.11116
40	9	0	−1.69478	−2.23949	−1.0861
41	6	0	2.770124	−0.57065	−0.47451
42	6	0	−5.52606	−0.19307	−0.20082
43	6	0	−5.15208	1.088887	−0.51057
44	6	0	−3.76746	1.31344	−0.6284

45	6	0	−3.04382	0.168319	−0.41087
46	16	0	−4.1005	−1.17626	−0.06867
47	9	0	−6.04139	2.079087	−0.69314
48	6	0	−7.2344	−1.99441	0.303051
49	6	0	−8.62001	−2.213	0.408289
50	6	0	−9.35103	−1.07249	0.156726
51	16	0	−8.28267	0.262758	−0.2092
52	9	0	−6.35039	−2.97854	0.511326
53	6	0	−6.86103	−0.71934	−0.02333
54	6	0	−1.5848	0.016624	−0.41176
55	6	0	−12.9148	0.388875	−0.04888
56	6	0	−11.499	0.294745	−0.08346
57	6	0	−10.813	−0.9369	0.178893
58	6	0	−11.6418	−2.00812	0.454273
59	6	0	−13.0432	−1.91532	0.495642
60	7	0	−13.5245	1.577672	−0.32613
61	6	0	−12.787	2.608905	−0.60584
62	6	0	−11.3626	2.512224	−0.62599
63	7	0	−10.7496	1.391629	−0.37537
64	9	0	−11.1573	−3.22391	0.718242
65	9	0	−13.6868	−3.04936	0.786692
66	6	0	−17.6404	−1.17161	0.150937
67	6	0	−17.3567	0.082789	0.592883
68	6	0	−15.976	0.380742	0.688445
69	6	0	−15.1964	−0.68378	0.316005
70	16	0	−16.1898	−2.04257	−0.14276
71	9	0	−18.2915	0.980444	0.917346
72	6	0	−13.7306	−0.74815	0.255808
73	8	0	14.2872	3.770907	−0.19881
74	6	0	15.68097	3.472335	−0.23425
75	8	0	−10.6998	3.628842	−0.91808
76	6	0	−9.27514	3.548408	−0.95369
77	8	0	−0.8313	4.425513	1.047384
78	6	0	−2.24341	4.614602	1.055951
79	1	0	11.73571	4.082016	−0.16199
80	1	0	18.38402	−1.15494	−0.33433

81	1	0	14.83732	−3.17195	1.127871
82	1	0	9.02681	2.057397	1.086032
83	1	0	2.936088	−2.5599	−1.36376
84	1	0	1.688453	3.856085	0.93413
85	1	0	−3.3324	2.275068	−0.84848
86	1	0	−9.0326	−3.17545	0.65997
87	1	0	−13.2686	3.556109	−0.83284
88	1	0	−18.6108	−1.62088	0.005616
89	1	0	−15.5888	1.338898	0.997936
90	1	0	16.18399	4.437291	−0.27181
91	1	0	15.98199	2.913488	0.655475
92	1	0	15.92426	2.880049	−1.12015
93	1	0	−8.93484	4.550911	−1.20756
94	1	0	−8.87893	3.243849	0.017992
95	1	0	−8.94588	2.830089	−1.70829
96	1	0	−2.40233	5.604707	1.480091
97	1	0	−2.73712	3.850193	1.660977
98	1	0	−2.64346	4.572362	0.038642

7. References

S1. S. Olivieri, R. Tarroni, N. Della Ca', R. Mancuso, B. Gabriele, G. Spadoni and C. Carfagna, *Adv. Synth. Catal.*, 2020, **362**, 533–540.

S2. M. J. Frisch, G. W. Trucks, H. B. Schlegel, G. E. Scuseria, M. A. Robb, J. R. Cheeseman, G. Scalmani, V. Barone, G. A. Petersson, H. Nakatsuji, X. Li, M. Caricato, A. V. Marenich, J. Bloino, B. G. Janesko, R. Gomperts, B. Mennucci, H. P. Hratchian, J. V. Ortiz, A. F. Izmaylov, J. L. Sonnenberg, D. Williams-Young, F. Ding, F. Lipparini, F. Egidi, J. Goings, B. Peng, A. Petrone, T. Henderson, D. Ranasinghe, V. G. Zakrzewski, J. Gao, N. Rega, G. Zheng, W. Liang, M. Hada, M. Ehara, K. Toyota, R. Fukuda, J. Hasegawa, M. Ishida, T. Nakajima, Y. Honda, O. Kitao, H. Nakai, T. Vreven, K. Throssell, J. A. Montgomery Jr., J. E. Peralta, F. Ogliaro, M. J. Bearpark, J. J. Heyd, E. N. Brothers, K. N. Kudin, V. N. Staroverov, T. A. Keith, R. Kobayashi, J. Normand, K. Raghavachari, A. P. Rendell, J. C. Burant, S. S. Iyengar, J. Tomasi, M. Cossi, J. M. Millam, M. Klene, C. Adamo, R. Cammi, J. W. Ochterski, R. L. Martin, K. Morokuma, O. Farkas, J. B. Foresman and D. J. Fox, *Gaussian 16, Revision C.02*; Gaussian, Inc., Wallingford, CT, 2019.

S3. J. Kang, S. Y. Kim, H. H. Jo and K. Zong, *ChemSusChem*, 2024, **17**, e202400216.

S4. W. He, Q. Liu, S. Otep, H. Matsumoto, S. Manzhos, P. Sonar, A. K. K. Kyaw and T. Michinobu, *Chin. J. Chem.*, 2023, **41**, 1028–1036.

S5. J. Mai, T.-K. Lau, J. Li, S.-H. Peng, C.-S. Hsu, U.-S. Jeng, J. Zeng, N. Zhao, X. Xiao and X. Lu, *Chem. Mater.*, 2016, **28**, 6186–6195.

S6. P. Yin, Y. Ma and Q. Zheng, *J. Mater. Chem. A*, 2022, **10**, 10400–10407.
S7. R. Po, G. Bianchi, C. Carbonera and A. Pellegrino, *Macromolecules*, 2015, **48**, 453–461.
S8. J. Kimpel, Y. Kim, J. Asatryan, J. Martín, R. Kroon and C. Müller, *Chem. Sci.*, 2024, **15**, 7679–7688.
S9. J. J. Rech, J. Neu, Y. Qin, S. Samson, J. Shanahan, R. F. Josey, H. Ade and W. You, *ChemSusChem*, 2021, **14**, 3561–3568.